Global Change Biology

WILEY

Global Change Biology

RESEARCH ARTICLE OPEN ACCESS

A Simple Stomatal Model That Unifies the Metabolic and Hydraulic Control of Carbon and Water Flux

Thomas N. Buckley[1] | Julien Lamour[2] | David M. Barnard[3] | Daniel W. Buckley[4] | Andrew J. Jarvis[5] | Antonio Diaz-Espejo[6] | Alistair Rogers[7] | Lawren Sack[8]

[1]Department of Plant Sciences, University of California, Davis, Davis, California, USA | [2]Centre de Recherche sur la Biodiversité et l'Environnement (CRBE), Université de Toulouse, CNRS, IRD, Toulouse INP, Université Toulouse 3—Paul Sabatier (UT3), Toulouse, France | [3]USDA Agricultural Research Service, Water Management and Systems Research Unit, Fort Collins, Colorado, USA | [4]Gar-Field High School, Woodbridge, Virginia, USA | [5]Lancaster University, Lancaster, UK | [6]Plant Ecophysiology and Irrigation Group, Instituto de Recursos Naturales y Agrobiología de Sevilla (IRNAS, CSIC), Sevilla, Spain | [7]Climate & Ecosystems Sciences Division, Lawrence Berkeley National Laboratory, Berkeley, California, USA | [8]Department of Ecology and Evolutionary Biology, University of California, Los Angeles, California, USA

Correspondence: Thomas N. Buckley (tnbuckley@ucdavis.edu)

Received: 30 December 2025 | **Revised:** 1 June 2026 | **Accepted:** 29 June 2026

Keywords: drought | hydraulic | model | photosynthesis | stomata | transpiration

ABSTRACT

A striking incongruity has long persisted in the modeling framework typically used to predict CO_2 and water vapor exchange between land plants and the atmosphere across scales. Generally, photosynthetic CO_2 demand is estimated using process-based models of biochemistry, but the biophysical stomatal constraint on photosynthesis and transpiration (g_{sw}) is estimated using "black box" empirical or optimization-based models. Empirical models of g_{sw} can only be parameterized in the domain of the training data, limiting confidence in predictions made outside that domain; optimization-based models rely on eco-evolutionary "goal functions" about which there remains poor consensus. To resolve this incongruity, we present a novel process-based model for g_{sw} with parameters that all have biophysical meaning, and of which only two require empirical fitting, thus ensuring tractability for application in land-surface models (LSMs). The model successfully reproduces variation in g_{sw} diurnally, globally, and in relation to soil drought and when drought and heat co-occur. The model also has greater functionality than previous models, by predicting stomatal closure under soil drought, the effect of variations in soil-leaf hydraulic conductance, stomatal closure in response to soil and atmospheric drought in darkness, and stomatal opening at high temperatures in both low and high light. With structure and parameters based on physiological processes, this model can translate continuing improvement in understanding of underlying biophysical and molecular genetic causes into predictions for carbon and water exchange, offering greater confidence for predicting the influence of stomata on land-surface exchanges of mass and energy in future climates.

1 | Introduction

Leaf stomata are a dominant control on CO_2, energy, and water vapor exchanges between the vegetated land surface and the atmosphere. Stomatal aperture, and hence diffusive conductance (g_{sw}, mol m^{-2} s^{-1}; symbols are defined in Table 1), varies dynamically in response to shifts in many environmental conditions, including irradiance, CO_2 concentration, temperature, evaporative demand, and soil water potential. However, g_{sw} can differ among plants exposed to different environmental conditions or experimental manipulations, notably atmospheric CO_2 enrichment (Ainsworth and Long 2005; Ainsworth and Rogers 2007). g_{sw} can also vary among leaves of the same plants when other traits differ, such as photosynthetic capacity (Wong et al. 1979) or hydraulic conductance (Brodribb et al. 2002). g_{sw} thus varies widely over time, within ecosystems, and across the

TABLE 1 | List of parameter and variables used in the main text.

Description	Symbol	Units	Default value
Parameters and variables used in the new model (Equation 3)			
Net CO_2 assimilation rate	A	$\mu mol\, m^{-2} s^{-1}$	—
CO_2-saturated assimilation rate	A_m	$\mu mol\, m^{-2} s^{-1}$	—
Bioenergetic capacity for stomatal opening	b	$\mu mol\, m^{-2} s^{-1}$	—
Value of b in darkness	b_o	$\mu mol\, m^{-2} s^{-1}$	0.3
Leaf to air water vapor mole fraction difference	Δw	$mmol\, mol^{-1}$	10
Soil-leaf hydraulic conductance (at 25°C)	$K_{(25)}$	$mmol\, m^{-2} s^{-1} MPa^{-1}$	3
Leaf boundary layer resistance to CO_2	r_{bc}	$m^2\, s\, mol^{-1}$	0
Rate of non-photorespiratory CO_2 release (at 25°C)	$R_{d(25)}$	$\mu mol\, m^{-2} s^{-1}$	0.5
Stomatal scaling and sensitivity coefficient	s	$mol\, \mu mol^{-1} MPa^{-1}$	0.02
Stomatal closure point	ψ_c	MPa	−2
Soil water potential	ψ_s	MPa	0
Parameters used in the simplified form of the new model (Equation 5)			
Maximum transpiration rate ($K(\psi_s - \psi_c)$)	E_m	$mmol\, m^{-2} s^{-1}$	6
Composite parameter (K/s)	p	$nmol\, m^{-2} s^{-1}$[a]	150
Other parameters and variables used in the main text			
Guard cell hydroactive advantage	α	—	—
Sensitivity of $\delta\pi_g$ to τ and P_e	β	$[mmol\ ATP\ m^{-2}]^{-1}$	—
Intercellular CO_2 mole fraction	c_i	$\mu mol\, mol^{-1}$	—
Ambient CO_2 mole fraction	c_a	$\mu mol\, mol^{-1}$	425
Proportionality factor used in BMF model	χ	$mol\, m^{-2} s^{-1} MPa^{-1}$	—
Leaf to air vapor pressure difference (VPD)	D	kPa	1
Slope parameter	g_1	$kPa^{0.5}$ or unitless[b]	2.89 or 10.22
Intercept parameter	g_0	$mol\, m^{-2} s^{-1}$	0.018
Photorespiratory CO_2 compensation point	Γ_*	$\mu mol\, mol^{-1}$	—
Relative humidity	h	—	0.684
Potential electron transport rate	J	$\mu mol\, m^{-2} s^{-1}$	—
Net epidermal mechanical advantage	M	—	—
Epidermal turgor pressure	P_e	MPa	—
Guard cell turgor pressure	P_g	MPa	—
Epidermal osmotic pressure	π_e	MPa	—
Penalty function in hydraulic penalty (HP) models	Θ	—	—
Leaf temperature	T	°C	25
[ATP] of photosynthetic cells	τ	$mmol\ ATP\ m^{-2}$	—

[a]The units $nmol\, m^{-2} s^{-1}$ are equivalent to those of K ($mmol\, m^{-2} s^{-1} MPa^{-1}$) divided by those of s ($mol\, \mu mol^{-1} MPa^{-1}$).
[b]g_1 has units of $kPa^{0.5}$ in the USO model, and no units in the BB model.

Earth's surface, which presents a fundamental challenge for any attempt to represent the stomatal constraint on surface-atmosphere exchange, in particular within land surface models (LSMs) (Franks et al. 2017; Rogers et al. 2017) nested within the Earth system models used in climate change research. Because stomata can profoundly affect large scale surface-atmosphere exchange (Berry et al. 2010; Hetherington and Woodward 2003), an accurate representation of their responses to the environment

is essential, particularly under future climate scenarios where conditions and plant responses may differ markedly from the present.

Current LSMs rely on empirical or optimization-based models of g_{sw}. The most widely used such models are the Ball-Berry model (BB; Ball et al. 1987) (Equation 1) and the Unified Stomatal Optimization model (USO; Medlyn et al. 2011) (Equation 2), which share a similar structure:

$$g_{sw} = g_0 + g_1 \frac{hA}{c_a}, \tag{1}$$

$$g_{sw} = g_0 + \left(1 + \frac{g_1}{\sqrt{D}}\right)\frac{1.6A}{c_a}. \tag{2}$$

These models represent the short-term variation in g_{sw} due to changes in the leaf environment, including ambient CO_2 mole fraction (c_a), relative humidity (h) or vapor pressure deficit (D), and leaf net CO_2 assimilation rate (A). Each model depends on two empirical parameters: g_0, which represents the value of g_{sw} when $A = 0$ (e.g., at the photosynthetic light compensation point), and g_1, which represents the sensitivity of g_{sw} to assimilation rate and environmental conditions. To predict g_{sw} solely from environmental conditions, one must also constrain the value of A in Equations (1) or (2), which requires additional inputs needed to drive a biochemical model for CO_2 assimilation rate, including temperature, light intensity, and photosynthetic parameters, possibly including mesophyll conductance; these "hidden" variables impact g_{sw} even when g_0 and g_1 are constants. At longer time scales of seasons to years, the parameters g_0 and g_1, as well as the photosynthetic parameters, can change substantially; thus, LSMs must update these parameters empirically to capture acclimation of leaf gas exchange to seasonality, e.g., in temperature and soil drought.

The BB model was based on empirical observations of the relationship between g_{sw} and A when environmental conditions (CO_2, light, relative humidity, and temperature) were varied, and has been widely used due to its combination of simplicity and performance. By contrast, the USO model was derived partly from Cowan and Farquhar (1977) optimization theory (CF), which posits that stomata respond to environmental fluctuations in a way that maximizes photosynthesis, given limits on water availability for transpiration. This theoretical basis in eco-evolutionary optimization theory has placed USO on firmer ground, epistemically, than the more empirical BB model, and as a result, USO has progressively replaced BB for applications in LSMs (De Kauwe et al. 2015; Franks et al. 2018; Li et al. 2022). Since the publication of the USO model, many other optimality-based models have been published, based on a range of different formulations of the evolutionary "goal function" that stomatal behavior putatively seeks to maximize (Dewar et al. 2022; Eller et al. 2018; Prentice et al. 2014; Sabot et al. 2022; Wolf et al. 2016), reviewed by Wang et al. (2020).

Each of these modeling approaches has significant drawbacks. These include the inability to predict some features of stomatal behavior under certain conditions, difficulty in interpretation of goodness-of-fit measures, incoherence in the underlying epistemic basis, and lack of consensus about how the approach should be applied (Table 2). In our view, however, the most important drawback of these approaches is that they are not based on current understanding of the physiological processes underlying stomatal responses. A model for stomatal conductance whose mathematical structure is transparently based on biophysical processes, and which is also analytical (i.e., not requiring iterative numerical solution, which multiplies computational costs), would have great value to the modeling community. Firstly, because the parameters in such a model would have explicit biophysical meaning, it should be far easier to predict and understand how they vary among species and environments and over time, and how they should relate to other more fundamental traits of anatomy and physiology and to species' genetics. In some cases, process-based parameters can be measured directly by experiment, rather than requiring empirical parameterization through the model itself (as is required for the parameters g_0 and g_1 in the USO and BB models). Even when process-based model parameters are obtained by fitting the model to data rather than by direct measurement, the parameters remain biologically interpretable because the model is grounded in known biophysical mechanisms. Secondly, process-based models are more readily generalized, and improved by increasing knowledge of physiological mechanisms, than empirical models, which increases confidence in their predictions when applied beyond the domain of calibration, such as under future climate scenarios.

At present, there is a strong consensus about two general features of the mechanisms of stomatal function, which form the foundation for a useful process-based model of g_{sw}. First, in most land plants, responses involving factors that influence leaf water status, such as soil moisture, evaporative demand and plant hydraulic conductance, are largely mediated by physiologically active sensing of water status somewhere within the leaf itself; this is often called the "hydroactive" response (Buckley 2005, 2019; McAdam and Brodribb 2016). The exact identity and location of the sensor(s) of water status are not certain (Buckley 2019; Kuromori et al. 2014; McAdam and Brodribb 2018). Second, responses involving factors that influence photosynthetic processes (e.g., irradiance, CO_2 concentration and temperature) are largely, though not entirely, mediated by signals from chloroplasts—likely in photosynthesizing mesophyll cells but possibly also in guard cells themselves—and these signals result in regulation of g_{sw} in proportion to the balance between energy supply from the light reactions and energy consumption by the Calvin cycle (Busch 2014; Lawson 2009; Lawson et al. 2018; Lawson and Matthews 2020; Messinger et al. 2006; Mott 2009). The precise sensor is not yet known, but may involve the redox state of plastoquinone (Busch 2014). There are also guard cell-endogenous responses to blue light and CO_2 independent of photosynthesis, though these may contribute only a minor portion of changes in stomatal conductance in intact leaves in nature (Messinger et al. 2006; Mott 2009).

The basic existence and importance of these water status- and photosynthesis-linked stomatal responses have been widely appreciated for decades, yet these have not been integrated in

TABLE 2 | Drawbacks of stomatal conductance models currently in wide use.

Model(s) affected	Description of drawback	Resolution in the new model
BB, USO	The models do not natively predict stomatal responses to soil water potential (ψ_s) or soil-leaf hydraulic conductance (K), in contrast to observations (Comstock and Mencuccini 1998; Saliendra et al. 1995). Soil drought responses can only be predicted by augmenting the models with secondary empirical functions.	Because the new model is based on the hydroactive response of stomata, it natively predicts responses to any factor that influences leaf water status, including ψ_s and K.
BB, USO	The models predict positive responses of stomatal conductance to increasing evaporative demand and CO_2 concentration in darkness, whereas the opposite is observed experimentally (Barbour and Buckley 2007; Cavender-Bares et al. 2007; Messinger et al. 2006).	The new model predicts the linkage between photosynthesis and stomatal function not by assuming g_{sw} is proportional to A, but instead, by assuming stomata sense some measure of the balance between the supply of photosynthetic energy from the light reactions and its consumption by the Calvin cycle. This captures observed nonlinearity, and leads to correct predictions of stomatal behavior in darkness and in plants with genetically modified photosynthetic properties.
BB, USO, HP	The link between photosynthesis and stomatal function is predicted by assuming g_{sw} increases whenever A increases and vice versa, all else equal. This fails to predict the effect of Rubisco suppression on stomatal conductance (von Caemmerer et al. 2004), and the fact that whereas A typically decreases at high temperatures, g_{sw} often continues to increase (Diao et al. 2024; Mills et al. 2024; Urban et al. 2017).	
BB, USO	The assumption of a linear relationship between g_{sw} and A often fails, particularly at low (Ball 1988; Barnard and Bauerle 2013) and high light intensities (Deans et al. 2020; Lamour et al. 2022). This makes fitted parameter values sensitive to the particular range of conditions used during parameterization (Kromdijk et al. 2019; Lamour et al. 2022) and potentially biases comparisons of species differing in photosynthetic capacity (Lamour et al. 2023).	
BB, USO	Goodness-of-fit parameters (e.g., r^2) can be misleading, both because of shared error in concurrent measurements of A (which is used to predict g_{sw}) and g_{sw} (measurements of which are used to test the model), and because g_{sw} and A are mathematically co-determined (Aphalo and Jarvis 1993; Brett 2004; Lloyd et al. 2013).	Although A appears in the new model, as in BB and USO, its partial derivative with respect to A is negative rather than positive, which artefactually deflates rather than inflates goodness-of-fit parameters.
USO	When photosynthesis is light-saturated, the model's predictions diverge radically from the optimality theory (Cowan and Farquhar 1977) on which the model is ostensibly based. The authors posited that stomata cannot identify the optimum in high light, and thus always behave as if photosynthesis were light-limited; yet, it seems incongruous to posit that evolution has optimized stomatal function in low light while leaving stomatal behavior highly sub-optimal in high light (Buckley et al. 2017).	The new model makes no assumptions about the adaptive significance of stomatal function, including that stomatal responses are in any sense "optimized." Thus, it avoids each of these issues.
USO	The key economic parameter tying the model to optimization theory, the marginal carbon revenue of water ($\partial A / \partial E$), is not itself predicted by the theory and instead must be estimated empirically.	
HP	There is no consensus about the appropriate form of the hydraulic penalty function (Θ) (Wang et al. 2020), so Θ varies among models and omits some considerations that influence hydraulic risk, such as parameters of stomatal, hydraulic and thermal kinetics (Buckley et al. 2023).	

(Continues)

TABLE 2 | (Continued)

Model(s) affected	Description of drawback	Resolution in the new model
LC	The model's goal function (the ratio of A to a weighted sum of transpiration rate and carboxylation capacity) assumes the only cost of sustaining transpiration and photosynthetic protein function is maintenance respiration, thus omitting other costs that may be far greater, such as building and replacing the tissues that acquire water and nitrogen and transport them to leaves.	
USO, HP, LC	Because optimality does not predict some important features of stomatal behavior, such as nocturnal opening, finite conductance in the absence of evaporative demand, and insensitivity to evaporative demand in many tropical species (Domingues et al. 2014; Lombardozzi et al. 2017), its use to predict g_{sw} is questionable.	

Abbreviations: BB, Ball-Berry model (Ball et al. 1987); HP, hydraulic penalty models (Eller et al. 2018; Sperry et al. 2017; Wang et al. 2020; Wolf et al. 2016); LC, Least-Cost theory (Prentice et al. 2014); USO, Unified Stomatal Optimisation model (Medlyn et al. 2011).

LSMs. Indeed, Farquhar and Wong (1984) proposed a model for g_{sw} based on photosynthetic energy balance (mediated specifically by mesophyll ATP concentration), and the hydroactive response was incorporated in stomatal models at least as early as the 1970s (Delwiche and Cooke 1977). Both Dewar (1995, 2002) and Jarvis and Davies (1998) proposed representations of photosynthetic energy balance in models of g_{sw}. Buckley et al. (2003) synthesized both ideas to produce a model (the "BMF" model) that was consistent with contemporary understanding of stomatal hydromechanics and plant water relations, and which incorporated the Farquhar and Wong ATP model; however, the BMF model is analytically complex and contains parameters too difficult to measure widely enough to enable broad application. Buckley et al. (2012) suggested a simplification that replaced the ATP submodel with an empirical model for the stomatal response to light, a formulation which has been applied particularly in hydrological modelling (Liu et al. 2022; Liu, Buckley, et al. 2019; Liu, Wang, et al. 2019)—yet, its broader utility is limited by the fact that it does not predict a CO_2 response and is not explicitly coupled to photosynthesis. Thus, there remains no process-based integrated model of stomatal conductance and photosynthesis that includes both the hydroactive response and the effect of photosynthetic energy balance, yet is sufficiently compact and analytically soluble to be useful in LSMs.

We propose a novel model that aims to fill this gap, and thereby to improve the representation of physiological processes controlling gas exchange in LSMs. This new model combines the hydraulic insights of the BMF model with the semi-mechanistic treatment of photosynthetic energy balance suggested by Jarvis and Davies (1998), and which, like the BB and USO models, yields an analytical solution when combined with diffusional and biochemical constraints on CO_2 exchange. Also like BB and USO, the model contains two coefficients that require empirical calibration; however, in the proposed model, those coefficients have direct links to physiological and anatomical properties, which facilitates their interpretation and generalization to future conditions. The model natively predicts stomatal responses to changes in soil moisture and soil-leaf hydraulic conductance. We demonstrate the model's predictions, evaluate it by comparison with measurements, and compare its predictions with those of the USO and BB models.

2 | Methods

Here we propose the following model, whose structure arises from the same biophysical constraints and biological assumptions that underlie the process-based model of Buckley et al. (2003) (the "BMF" model, described in Appendix A.1), but with simplifications intended to facilitate application in ecophysiology and in LSMs while retaining a clear basis in underlying biophysical processes:

$$g_{sw} = \frac{sb\left(\psi_s - \psi_c\right)}{1 + sb\Delta w / K}, \tag{3a}$$

where s is a scaling and sensitivity coefficient (discussed below), ψ_s is soil water potential, ψ_c is the stomatal closure point (the leaf water potential at which stomata close, also discussed below), Δw is the leaf-to-air water vapor mole fraction difference, K is soil-leaf hydraulic conductance, and b is the bioenergetic potential for stomatal opening. b is the sum of two quantities: the residual photosynthetic capacity—that is, the CO_2-saturated assimilation rate at the current irradiance (A_m) minus the actual current assimilation rate (A)—and a basal level of b that persists in darkness (b_o):

$$b = A_m - A + b_o. \tag{3b}$$

The residual photosynthetic capacity is the amount by which A would increase if the limitation due to CO_2 were eliminated. It is equivalent to the product of A_m and the relative limitation of photosynthesis by CO_2 ($1 - A/A_m$, sensu Jones (1985)), and it captures the stomatal responses to light and CO_2, as well as part of the response to temperature. In C_3 species, $A_m = ¼J - R_d$, where J is the potential electron transport rate and R_d is the rate of non-photorespiratory CO_2 release; in C_4 species, and using the model of Collatz et al. (1992), A_m is computed from irradiance and carboxylation capacity (Equation S48).

2.1 | Rationale for Changes Adopted in Equation (3) From the BMF Model

i. *The bioenergetic potential for stomatal opening (b)—which is driven mainly by the residual photosynthetic capacity—replaces ATP concentration*. In the BMF model, ATP concentration (denoted τ) predicts the stomatal responses to light and CO_2. However, the signal that couples stomatal responses to photosynthetic processes remains unknown and is probably not τ itself (Busch 2014). By replacing τ with b, the new model captures the stomatal responses to light and CO_2 using only parameters that are typically already available to modelers—eliminating the need to estimate internal parameters in the ATP model (Appendix A.1). b also includes an offset parameter, b_o, which reflects the current understanding that the influence of leaf energy metabolism on stomatal conductance persists in darkness—often causing stomata to remain partly open at night (Bucci et al. 2004; Buckley et al. 2011; Fisher et al. 2007; Kavanagh et al. 2007; Zeppel et al. 2010). (Note that b_o predicts only the stomatal component, not the cuticular component, of nocturnal leaf conductance.)

ii. *The stomatal scaling and sensitivity coefficient (s) replaces two parameters in the BMF model (χ and β)*. To understand the parameter s in Equation (3), first note that the product sb is analogous to the product $\chi(\beta\tau - M)$ in the BMF model (see Appendix A.1). χ is defined by the relationship $g_{sw} = \chi(P_g - (1+M)P_e)$ (Equation A1), which describes how the turgor pressures of guard and epidermal cells (P_g and P_e, respectively) influence stomatal aperture; M is the net epidermal mechanical advantage. Thus, $s \approx (1/b) \times \chi(\beta\tau - M)$. Under conditions promoting stomatal opening, $\beta\tau \gg M$ (Buckley et al. 2003), so to a first approximation,

$$s \approx \chi\beta \times \frac{\tau}{b}. \quad (4)$$

Since τ and b capture the same effects (namely, the photosynthetically-mediated influences of light and CO_2 on stomata), and since τ, like the residual photosynthetic capacity and hence b, is expected to scale together with photosynthetic capacity (Farquhar and Wong 1984), those photosynthetic influences cancel in the ratio τ/b, such that τ/b does not represent any fundamental influence on s, other than minor differences in the shapes of the responses of τ and b to light and CO_2. Therefore, variation in s should be driven mainly by the biophysical influences of χ, which captures how the properties of one stomate scale up to whole-leaf stomatal conductance, and β, which captures the sensitivity of guard cell osmotic regulation to leaf water status, light and CO_2. The first of these influences—the scaling of single-stoma conductance to the leaf—is mostly determined by stomatal size and density, such that s should be proportional to stomatal density and to the square root of stomatal size, all else equal (Sack and Buckley 2016). It is less obvious how the second influence on s (that of β) should vary across taxa or environments. Some insight arises from the finding of Oren et al. (1999) that the stomatal sensitivity to VPD is highly conserved across taxa; Buckley et al. (2012) showed that Oren's result implies a conservative ratio between the light-saturated value of $\chi\beta\tau$ and plant hydraulic conductance, K. Since the light-saturated value of τ is controlled by photosynthetic capacity, which itself is strongly correlated with K (Brodribb et al. 2002; e.g., Brodribb and Feild 2000), this suggests β should be fairly conservative, leaving variation in s across taxa and environments to be driven mostly by variation in stomatal density and size (Liu et al. 2023).

iii. *Stomatal closure point (ψ_c) replaces epidermal osmotic pressure (π_e)*. The occurrence of π_e in the BMF model arose from its assumption that the guard cells sense water status via epidermal turgor pressure, P_e. In the decades since the BMF model was first published, understanding has greatly increased regarding both the mechanism and phenomenology of how leaf water status influences g_{sw}. It is now understood that stomata sense not turgor pressure per se, but something more closely related to cell or tissue volume or water content (Sack et al. 2018). Thus, although stomata may indeed tend to close at water potentials close to the turgor-loss point (ψ_{TLP}), which is determined by osmotic pressure, ψ_c may not simply equal ψ_{TLP} (Bartlett et al. 2014). Replacing π_e with ψ_c allows for species variation in ψ_c, while still enabling ψ_c to be estimated using measurements of ψ_{TLP}.

Notably, ψ_c is not a variable within the model, and it is not the same thing as leaf water potential, ψ_L; rather, it is a parameter that describes a particular limiting threshold for ψ_L (namely, the value causing incipient stomatal closure). Although ψ_L does not appear explicitly as a variable in Equation (3), ψ_L is nevertheless implicitly dynamic in the system of equations that gave rise to Equation (3), and it varies dynamically along with g_{sw}. If one wished to calculate the value of ψ_L, they could apply the value of g_{sw} predicted by the model to the hydraulic constraint on ψ_L (e.g., Equation A3).

2.2 | Estimating the Model's Parameters

In addition to the photosynthetic parameters needed to calculate A_m and A, Equation (3) contains four physiological parameters that need to be estimated to predict g_{sw}: s, b_o, K and ψ_c. Although s and b_o have physiological meanings, as discussed earlier, it is simplest to calibrate them empirically, for example by fitting Equation (3) to observations of g_{sw}. K and ψ_c can likewise be fitted in this manner, but they can also be estimated by direct experimental measurements, discussed below.

The simplest way to estimate ψ_c is benchtop drying—that is, allowing an illuminated, transpiring plant or branch to dehydrate gradually, ensuring near-equilibrium of water potential among its leaves, while periodically measuring g_{sw} by gas exchange and measuring ψ_L by sampling leaves; ψ_c is the value of ψ_L at which g_{sw} reaches zero, or some practical limit such as 95% decline in g_{sw}. ψ_c is often closely related to the turgor loss point (ψ_{TLP}), so one can also simply estimate ψ_c as ψ_{TLP}, which in turn can be found in the literature or determined rapidly by osmometry (Bartlett et al. 2014; Bartlett, Scoffoni, Ardy, et al. 2012; Bartlett, Scoffoni, and Sack 2012; Maréchaux et al. 2015).

The soil-leaf hydraulic conductance, K, is defined as the steady-state water flux through the plant per unit of driving pressure difference between the soil and canopy: that is, the symbol K refers to the quantity [water flux]/($\psi_s - \psi_L - \rho GH$), where ρGH is the hydraulic head (ρ being the density of water, G the gravitational acceleration, and H the canopy height). Note as well that, because liquid water flux must equal vapor-phase water flux (transpiration rate, E) on average and at steady-state, the soil-leaf hydraulic conductance can also be understood as the steady-state transpiration rate per unit of driving pressure difference. Literature estimates of K and its soil-to-root, root, stem and leaf components are widely available for many species (Mencuccini 2003; Tsuda and Tyree 2000; Wolfe et al. 2023). Whole-plant flux needed to calculate K can be estimated from eddy covariance or sap flux measurements (Poyatos et al. 2020; Wilson et al. 2001; Wood et al. 2024), or scaled up from gas-exchange measurements of individual leaves using canopy models (de Pury and Farquhar 1997; Leuning et al. 1995). ψ_s is often estimated as the value of ψ_L at pre-dawn (when transpiration is minimal) and combined with mid-day ψ_L to calculate K (e.g., Phillips et al. 2002; Wood et al. 2024); note that this assumes any water potential gradient between the bulk soil and roots has dissipated by dawn, which may not always hold true, particularly in periods of high evaporative demand (Caird et al. 2007; Forster 2014; Fricke 2019). ψ_s can also be measured directly using tensiometers or soil psychrometers (Whalley et al. 2013), or inferred from direct measurements of soil water content if soil moisture-release curves are available (Novick et al. 2022). Alternatively, if diurnal time series of ψ_L and ψ_s are available, then diurnal trends in K can likewise be computed; indeed, at least two LSMs—CLM (Community Land Model; Kennedy et al. 2019) and Noah-MP (Li et al. 2021)—now estimate water potential at sub-hourly scales.

Applying these calculations in the limit of zero water potential throughout the plant gives a theoretical maximal value of K (K_{max}). The actual hydraulic conductance at any given point in the flow pathway often declines from K_{max} as water potential declines, generating a "vulnerability curve" (typically expressed as a functional dependence of K on ψ; i.e., $K = K_{max} \times f_v(\psi)$, where f_v is a dimensionless function that declines from unity as ψ_L declines below zero). Since water potential declines as water moves along the transpiration stream, maximally rigorous calculation of water flux requires integration of the vulnerability curve along the transpiration stream (i.e., water flux $= \int_{\psi_s}^{\psi_L} K_{max} f_v(\psi) d\psi$) (e.g., Sperry et al. 2016). In practice, it is also common to approximate this integral with a single discrete step and a single value of water potential (i.e., water flux $\approx K_{max} f_v(\psi_L) \cdot (\psi_s - \psi_L)$), or with one step for each major component of the flow pathway (soil, roots, stem, leaves). Notably, however, applications of "hydraulic penalty" models in LSMs have been successful using whole-plant or organ-specific vulnerability curves (Eller et al. 2018, 2020; e.g., Sperry et al. 2017), suggesting the full integral approach may not be necessary. Thus, to calculate K at any given time, one first finds the value of ψ_L that satisfies hydraulic constraints $\left(\psi_L \approx \psi_s - g_{sw}\Delta w/K = \psi_s - g_{sw}\Delta w/\left[K_{max} f_v\left(\psi_L\right)\right]\right)$, and then applies that value to the vulnerability curve to calculate K. Because the function $f_v(\psi_L)$ is often transcendental in form (e.g., involving exponential functions), it is often impossible to solve this expression analytically for ψ_L, in which case it must be solved by numerical iteration. If information describing K vulnerability is not available, K may be treated as a constant and the other parameters in the model validated accordingly. Finally, note that K also depends on temperature, in a manner that varies across studies and between plant compartments (roots, stems, leaves), but is almost always a positive response (Mills et al. 2024, 2026); in models, K is often assumed to vary from its value at 25°C (K_{25}) in proportion to the inverse of the viscosity of water (i.e., $K = K_{25} \times \left[4.891 \times 10^{10} \times \exp\left(-4209 / T_K - 0.04527 \times T_K + 3.376 \times 10^{-5} \times T_K{}^2\right)\right]$, where T_K is temperature in kelvins).

2.3 | Alternative Model Expression for Empirical Parameterization When ψ_s Is Unavailable

When soil water potential is not available, the model can be parameterized empirically. However, the model then has five unknown parameters (s, ψ_s, ψ_c, K and b_o) but only three independent degrees of freedom among them, due to the model's structure, and this can lead to overfitting. An alternative formulation is thus needed for when ψ_s is unknown. Equation (3) can be rearranged as

$$g_{sw} = \frac{E_m b}{p + b\Delta w}, \tag{5}$$

where E_m and p are equivalent to $K(\psi_s - \psi_c)$ and K/s in Equation (3). Thus, one can apply the model using fitted values of E_m and p. E_m can be interpreted as the maximum transpiration rate (the limit of $E\left[= g_{sw}\Delta w = E_m / \{p / b\Delta w + 1\}\right]$ as Δw approaches infinity). p is the value of $b\Delta w$ at which $E = E_m/2$; thus, a large value of p means that more light (higher b) and/or greater evaporative demand (higher Δw) is needed to make E reach a given fraction of its theoretical maximum.

2.4 | Solving the New Model With Diffusional and Biochemical Constraints on Assimilation Rate

As for the USO and BB models, an analytical expression for g_{sw} is obtained by coupling the equations for g_{sw} with biophysical models of diffusion (Caemmerer and Farquhar 1981) and photosynthetic CO_2 demand (Farquhar et al. 1980). The result is a cubic expression for A (presented in Appendix A.2 and derived in Methods S1), which is then applied to Equation (3) to calculate g_{sw}. In certain limiting conditions, the solution is simpler than a cubic (see Appendix A.2). Notably, the result remains cubic when nonzero boundary layer resistance is allowed.

2.5 | Experimental Tests and Comparison With the USO and BB Models

We tested the model using three datasets: Dataset #1 ("tree crops under drought") to evaluate the model under progressive drought, Dataset #2 ("*combined drought and heat stress*") to compare the model's performance with USO during a heatwave imposed after sustained soil water deficit in a eucalypt, Dataset #3 ("global stomatal conductance database") to assess how the model's fitted parameters vary across diverse species and environmental conditions, and Dataset #4 ("tropical tree light-response curves") to compare the model's performance to

BB and USO at low and high irradiance. A brief summary of these datasets and associated simulation methods is provided here, and additional details are given in Methods S3.

Dataset #1 comprised diurnal timecourses of g_{sw} in irrigated (control) and reduced-irrigation (drought) conditions in grapevine (*Vitis vinifera*), olive (*Olea europea*), and almond (*Prunus dulcis*) in Spain, previously applied to the BMF model by Rodriguez-Dominguez et al. (2016). To apply Equation (3), we calculated K from measured water potentials and transpiration rates, and fitted s, ψ_c and b_o; for USO and BB, we fitted g_1 and g_0. We used adjusted r^2 to compare model performance while accounting for the different numbers of fitted parameters in each model. We compared two scenarios: with the model fitted separately for each treatment, or fitted to both treatments together.

Dataset #2 is an experiment assessing whole-plant gas exchange in response to a four-day heatwave imposed after soil water had been withheld for 1 month, in *Eucalyptus parramattensis*. These data were originally reported by Drake et al. (2018) and later applied by Sicangco et al. (2026) to assess the USO model's ability to predict gas exchange under combined drought and heat wave conditions in comparison with hydraulic-penalty-type optimization-based g_{sw} models. We used these data to compare Equation (3) with USO under these conditions.

Dataset #3 is the largest publicly available dataset of g_{sw} measurements. It includes more than 300 species from around the world and was previously applied to the USO model by Lin et al. (2015). We used the new model in the form given by Equation (5), fitting the parameters E_m and p. We assumed $b_o = 0$ (following Lin et al. (2015), who assumed $g_0 = 0$). As parameters for the biochemical photosynthesis model were not available in this dataset, we assumed light-limited conditions when applying Equation (5), because this enables estimation of b from A and c_i alone:

$$b \approx \frac{3\Gamma_* A}{c_i - \Gamma_*}, \tag{6}$$

where Γ_* is the photorespiratory CO_2 compensation point. (Equation (6) follows from applying $b = ¼J - R_d - A$ to the Farquhar et al. (1980) model under regeneration limitation (Equation S3) and assuming $R_d = 0$.) We estimated Γ_* from temperature (Bernacchi et al. 2001) and c_i from reported A, c_a and g_{sw}. We excluded C_4 species because b could not be estimated for them in this way. To avoid overfitting, we also excluded species × site combinations with fewer than four points; this left 140 species × site combinations, representing 133 species and 57 sites. See Methods S3 for additional details.

Dataset #4 comprised light-response curves for three tropical tree species collected by Lamour et al. (2022). We used these data to test whether Equation (3) predicts the curvilinear relationship often observed between g_{sw} and A at low and high irradiances, in contrast to the BB and USO models, which always predict a linear relationship for given c_a and h or Δw, respectively.

2.6 | Simulation Procedures

We simulated generic responses to environmental factors using default parameter values given in Table 1, and except where otherwise noted, computed photosynthetic parameters and temperature responses following Bernacchi et al. (2003; 2001), as described in Methods S4. All calculations were performed in R. When comparing Equation (3) with BB and USO under generic conditions, we used numerical iteration to find the values of g_1 and g_0 that forced BB and USO to predict the same g_{sw} as Equation (3) in darkness and in high light (PPFD = 1000 μmol m^{-2} s^{-1}), with $\Delta w = 15$ mmol mol^{-1}, $c_a = 425$ μmol mol^{-1} and $T = 25$°C, under default values for other parameters. In all cases except Dataset #2, we set leaf boundary layer resistance to CO_2 (r_{bc}) to zero for simplicity; for Dataset #2, r_{bc} was needed to compute CO_2 and carbon fluxes for comparison with values measured in intact plants using whole-tree chambers, and we calculated it from wind speed and leaf size, as described in Methods S4.

3 | Results

3.1 | Generic Predictions of the New Model (Equation 3)

Equation (3) predicts the familiar short-term stomatal responses to light, evaporative demand, and ambient CO_2 (Figure 1a–c), as well as stomatal closure in response to declining soil water potential (Figure 1d). It also predicts interactions between different responses and parameters. For example, the light-saturated value of g_{sw} scales with photosynthetic capacity (Figure 1a), the CO_2 response is more sensitive in low light than in high light (Figure 1b), and the Δw response is more sensitive when K is small than when K is large (Figure 1c). Importantly, if K is made to decline concurrently with soil water potential (ψ_s), as often occurs during soil drought, a nonlinear response of g_{sw} to ψ_s is predicted (red line in Figure 1d).

3.2 | Tests in Tree Crops Under Drought (Dataset #1)

For Dataset #1, Equation (3) performed similarly to the USO and BB models if separate parameter values were fitted for each treatment (adjusted $r^2 = 0.75$–0.98 for the new model, vs. 0.78–0.97 for USO and 0.47–0.97 for BB; Table S1; Figure 2a,c,e), but strongly outperformed both USO and BB if a single set of parameter values were fitted for both treatments (adjusted $r^2 = 0.71$–0.98 for the new model, vs. 0.033–0.19 for USO and −0.064–0.14 for BB; Table S1; Figure 2b,d,f).

3.3 | Tests Under Combined Drought × Heatwave Conditions (Dataset #2)

Both the new model and the USO model satisfactorily reproduced effects of temperature on canopy photosynthesis and transpiration under control conditions (Figure 3a,c). Measured photosynthesis showed a weak overall decline at high temperature in the control while modeled rates peaked at between 25°C and 30°C (Figure 3a); in the heatwave-affected trees, photosynthesis again peaked at between 25°C and 30°C but declined strongly, approaching zero between 40°C and 45°C, and both models predicted similar patterns (Figure 3b). Measured transpiration rose with temperature below 30°C and remained

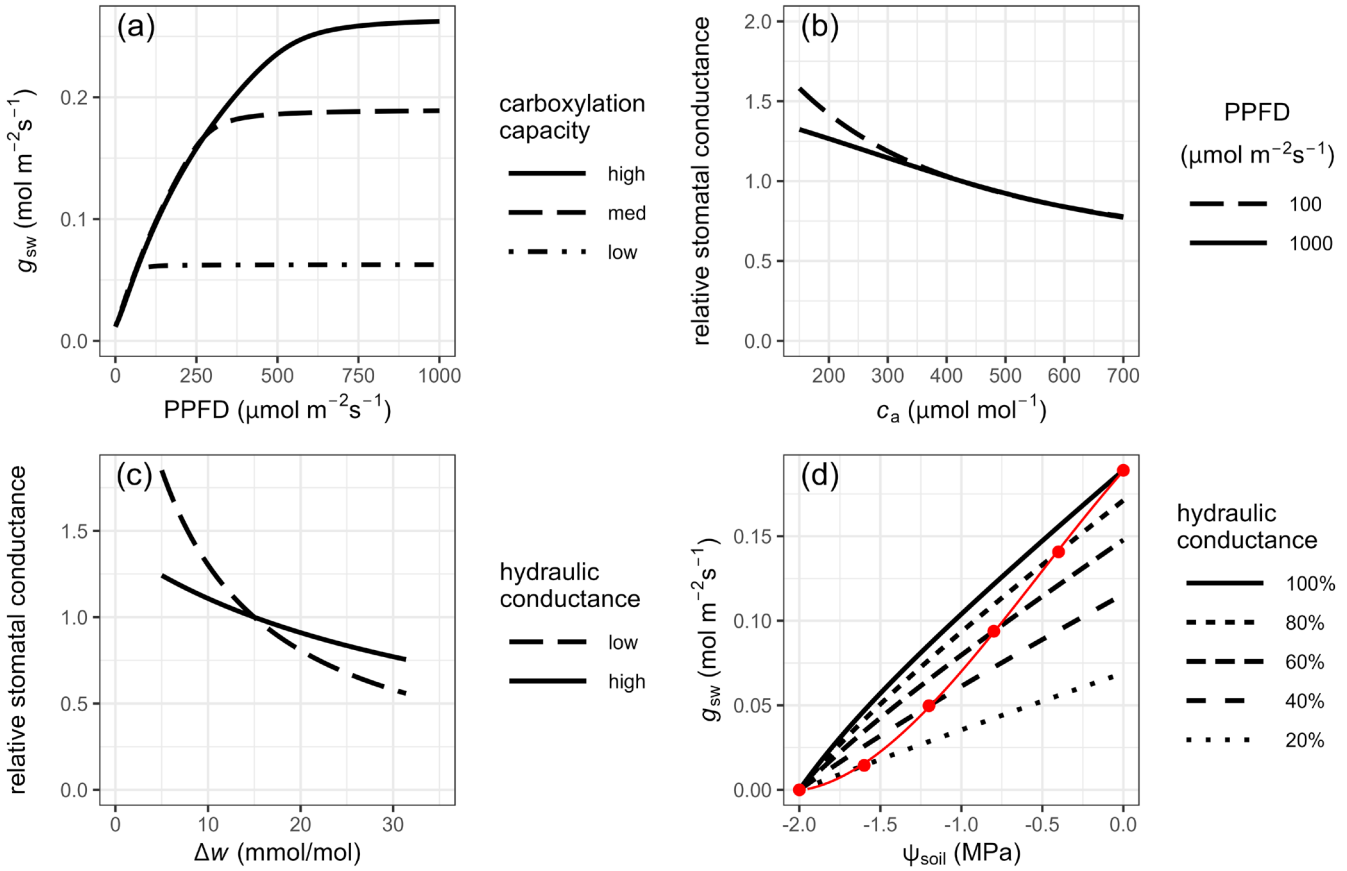

FIGURE 1 | Responses of stomatal conductance to environmental parameters, predicted by the model presented in this study. Responses to (a) photosynthetic photon flux density (PPFD) at three different carboxylation capacities (10, 50, and 100 μmol m^{-2}s^{-1}; electron transport capacity and respiration rate were also adjusted to maintain constant proportions with carboxylation capacity); (b) ambient CO_2 mole fraction (c_a) at two values of PPFD; (c) evaporative demand (Δw, the leaf to air water vapor mole fraction difference) for two values of soil-leaf hydraulic conductance (K; 1 and 5 mmol m^{-2}s^{-1}MPa^{-1}); and (d) soil water potential (ψ_s) at five different values of K (20%–100% of the default value of 3 mmol m^{-2}s^{-1}MPa^{-1}). In (b) and (c), stomatal conductance is expressed relative to its values at $c_a = 425$ μmol mol^{-1} and $\Delta w = 15$ mmol mol^{-1}, respectively, to facilitate comparison of the responses. In (d), the red symbols connected by a red curve are values of g_{sw} at $\psi_s = 0$, −0.4, −0.8, −1.2, −1.6 and −2.0 MPa, for progressively lower values of K (dashed lines), illustrating the response of g_{sw} to ψ_s that would occur if K declined concurrently with ψ_s.

steady or declined very weakly above that temperature; by comparison, the new model predicted a continuing rise (albeit weakly saturating) rise up to 45°C, whereas the USO model predicted a sharp decline above 30°C, reaching zero at around 44°C (Figure 3c,d). Both models satisfactorily predicted trends in midday leaf water potential in the control (Figure S1a); during the heatwave, the new model predicted midday water potentials satisfactorily, whereas the USO model greatly overestimated water potentials (Figure S1b).

3.4 | Tests Using Global Stomatal Conductance Database (Dataset #3)

When applied to Dataset #3, the new model (applied as Equation 5, with two fitted parameters [E_m and p] and assuming light-limited conditions so that b could be calculated from data available in the dataset of Lin et al. 2015) satisfactorily reproduced variation in g_{sw} (Figure 4); a linear regression of predicted vs. measured g_{sw} through all points combined gave $r^2 = 0.87$ for the new model (Figure 4a), vs. $r^2 = 0.90$ for the USO model (Figure 4b). Fitted values of E_m and p varied widely across biogeographic regions, evolutionary groups, and plant functional types (Figure 5, Table S2). In most cases, E_m, p and the USO slope parameter, g_1, varied in broadly similar fashion—being higher in non-woody than in woody plants, in warm than in cold environments, in angiosperms than in gymnosperms, and in humid than in semi-arid or dry-humid environments. Fitted values for both E_m and p were lowest in arctic environments, but this is partly an artefact of failed model fits (for five of eight arctic species, p equalled exactly 10^{-4}, the lower bound imposed in the fitting routine). We interpret these patterns, and deviations from general coordination of E_m, p and g_1, in Section 4.

3.5 | Tests Using Tropical Tree Light Response Curves (Dataset #4)

The relationship between the USO factor ($1.6A / \left[c_a\sqrt{D}\right]$, where D is VPD) and measurements of g_{sw} acquired during light response curves in three tropical tree species (previously reported

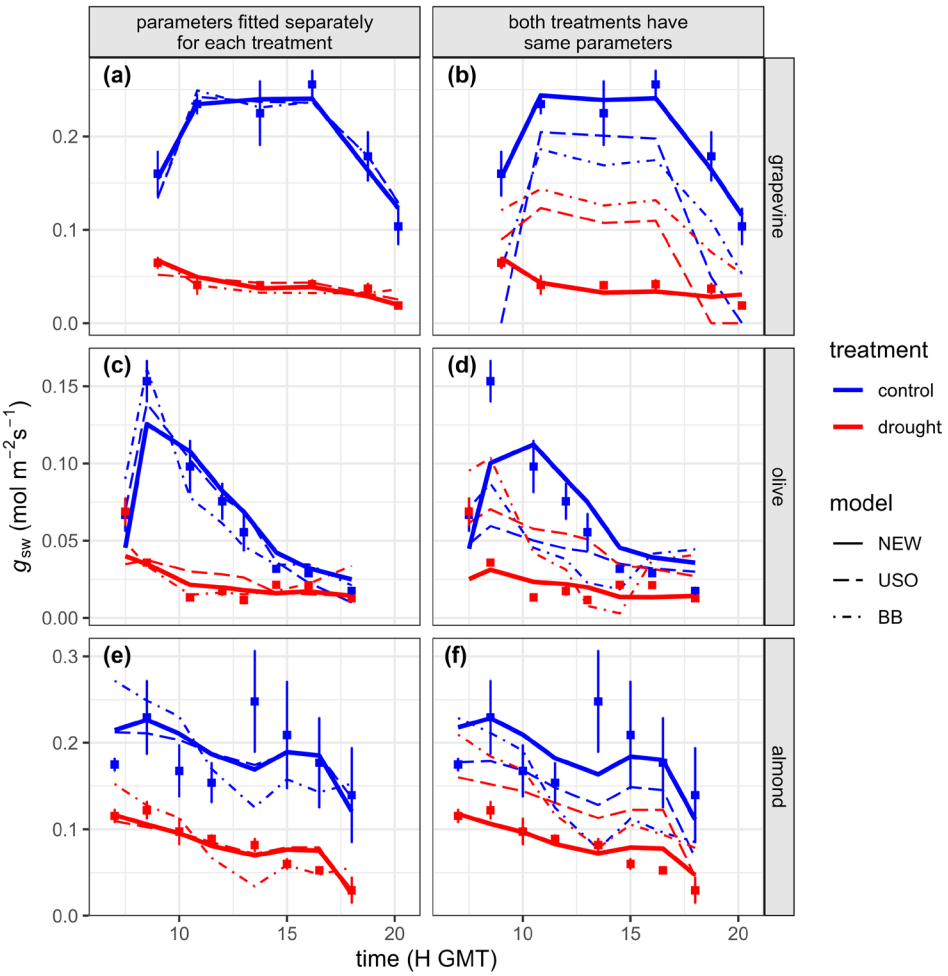

FIGURE 2 | Diurnal timecourses of stomatal conductance in *Vitis vinifera* (a, b), *Olea europea* (c, d), and *Prunus dulcis* (e, f), measured by gas exchange (symbols) and predicted by the new model (solid lines), USO (dashed lines) and BB (dash-dot lines), in control (blue) or soil drought (red) conditions. Error bars represent SEs over 3–4 plants per treatment. (a, c, e) Results with model parameters fitted separately for each treatment in each model; (b, d, f) results with a single value of model parameters fitted for both treatments combined.

by Lamour et al. 2022) was strongly nonlinear, with observed g_{sw} deviating more positively from the USO factor at high g_{sw} values (Figure 6a). By contrast, values of g_{sw} predicted by Equation (3) did not diverge from observations in this manner (Figure 6b). This is because the residual photosynthetic capacity (which performs the same function in the new model as the USO factor performs in the USO model) closely tracks the USO factor under RuBP regeneration-limited conditions, but diverges positively from the USO factor under carboxylation-limited conditions, thus making Equation (3) behave more like observed g_{sw} than like the USO model in high light.

4 | Discussion

The modeling community has lacked access to a model for g_{sw} whose structure is based on underlying physiological processes, yet is sufficiently compact and tractable, and hence computationally efficient, for application at large scales in land-surface models (LSMs). The g_{sw} models that currently dominate LSMs cannot natively predict effects of soil water deficit, and their parameters are challenging to relate to measurable and meaningful physiological processes (Table 2). The model presented here (Equation 3) has the potential to overcome these limitations. Its structure is based on well-established biophysical relationships of plant water relations and stomatal hydromechanics and physiology, or convenient approximations thereof. Two of its parameters—soil-leaf hydraulic conductance (K) and the stomatal closure point (ψ_c)—can be directly measured experimentally, while the other two—stomatal sensitivity (s) and the basal value of the bioenergetic capacity for stomatal opening (b_o)—can be estimated by fitting the model to data, while nonetheless having transparent links to physiological and anatomical processes. Because Equation (3) does not require iterative numerical solution—unlike other process-based models of stomatal conductance (e.g., Buckley et al. 2003; Hills et al. 2012)—it can more easily bridge the gap between stomatal physiology at the leaf scale and its impacts on carbon and water fluxes at large scales. In particular, it enables incorporation into LSMs of rapidly growing physiological understanding of the central role of plant hydraulics in ecosystem function (Anderegg, Konings, et al. 2018; Dukes et al. 2026; Torres-Ruiz et al. 2024; Wood et al. 2024), and of the tight coupling between stomatal and photosynthetic physiology (Lawson 2009; Lawson et al. 2018;

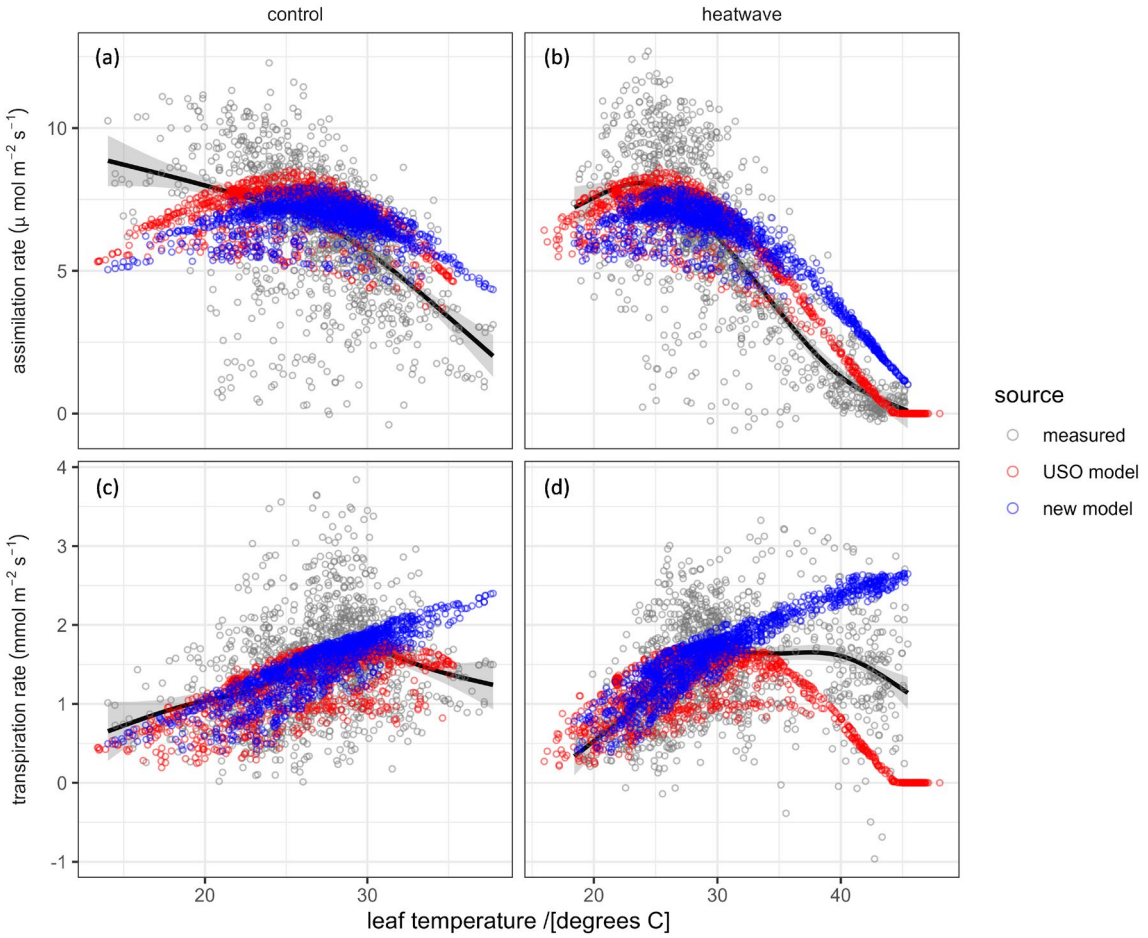

FIGURE 3 | Responses of CO_2 assimilation rate (a, b) and transpiration rate (c, d) to leaf temperature, under control conditions (a, c; daily max temperature 28°C–29°C) or during a four-day heatwave (b, d; daily max air temperature 43°C–44°C), measured for *Eucalyptus parramattensis* trees (grey symbols; black lines are GAMs fitted to the data with shading denoting ±95% confidence intervals) or simulated by the new model (blue symbols) or the USO model (red symbols). Soil water had been withheld from both control and heatwave trees for 30 days prior to the experiment. Original data from Drake et al. (2018), with USO simulations from Sicangco et al. (2026) (cf. their figure 5).

Lawson and Matthews 2020; Messinger et al. 2006; Mott 2009), while avoiding assumptions about the eco-evolutionary optimization of stomatal behavior (Table 2), as discussed below.

4.1 | Comparison With Existing Models Used in LSMs

Current LSMs mostly use one of two approaches to constrain g_{sw}: empirical models (e.g., BB) or "eco-evolutionary" optimization-based models (e.g., USO, hydraulic penalty models [HP; e.g., Wang et al. 2020; Eller et al. 2018; Wolf et al. 2016], or the "least-cost" theory [LC; Prentice et al. 2014]). These approaches have several drawbacks and limitations (Table 2). In BB, parameters require empirical estimation, and no currently articulated physiological or evolutionary principles predict their values or explain how they should be related to measurable biophysical traits. By contrast, the parameter g_1 in the USO model is related to the marginal carbon revenue of water $\left(\partial A/\partial E \equiv \left[\partial A/\partial g_{sw}\right]/\left[\partial E/\partial g_{sw}\right]\right)$; at time scales on which water supply can be treated as constant, the Cowan-Farquhar optimization theory (Cowan and Farquhar 1977) predicts that stomatal responses should keep $\partial A/\partial E$ constant and equal to some "target" value, $1/\lambda$. Thus, g_1 is conceptually related to water supply via CF theory. Yet CF provides no way to predict the value of λ, and in practice, g_1 remains an empirical parameter. In most HP models, the water-supply constraint is captured by assuming that stomatal behavior maximizes photosynthesis subject to a "penalty" (Θ) that scales with the loss of xylem hydraulic conductivity caused by embolism at low water potentials. However, stomatal closure during soil or atmospheric drought typically begins at much higher water potentials than those causing substantial embolism (Choat et al. 2018; Delzon and Cochard 2014; Scoffoni et al. 2018), and Θ should also be influenced by factors other than embolism (Buckley et al. 2023). Thus, there is no consensus regarding what form of Θ best represents eco-evolutionary optimization theory. Alternatively, the form and parameters of Θ can be treated empirically (Anderegg, Wolf, et al. 2018; Wolf et al. 2016), but that leaves the resulting models epistemically untethered, like BB. By contrast, the parameters of Equation (3) have a firm epistemic basis in physiological understanding. This does not preclude their empirical calibration, but it does provide a coherent rational framework for interpreting the calibrated values that result, and for understanding and predicting how they might covary across taxa and environments.

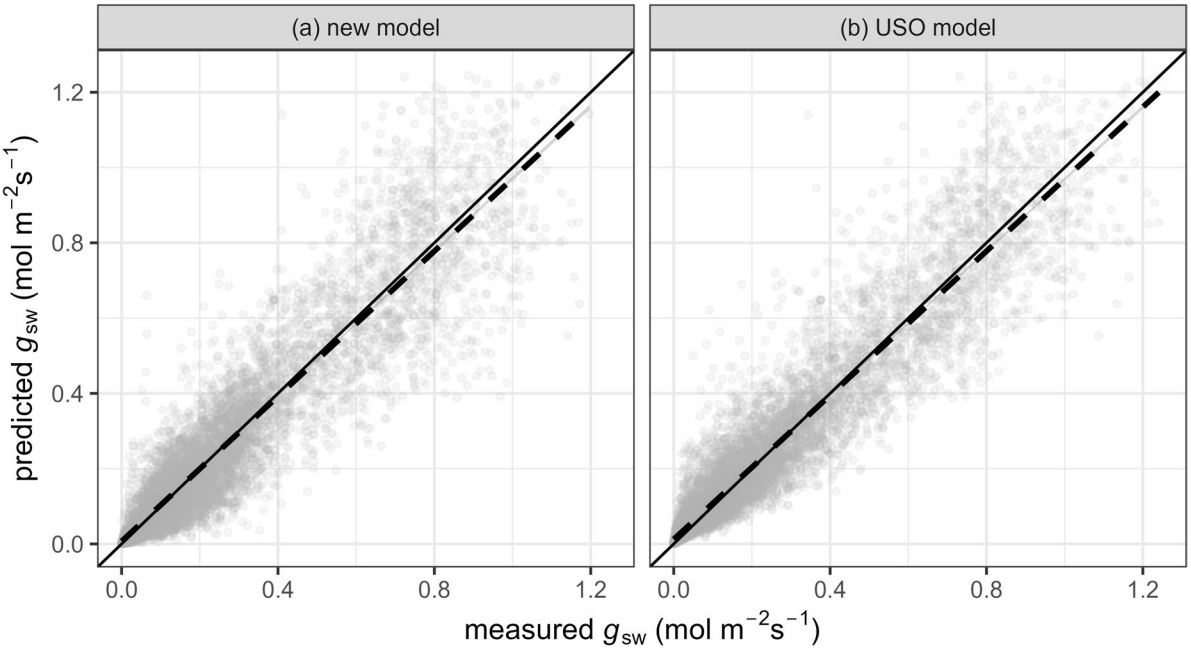

FIGURE 4 | Comparison of predicted vs. measured stomatal conductance, g_{sw} (data of Lin et al. 2015; Dataset #3), for (a) the new model (as Equation 5) and (b) the USO model (Equation 2) fitted separately to each species × site combination ($n = 140$) by adjusting the parameters E_m and p (Equation 5) and g_1 (Equation 2), with $g_0 = 0$ and $r_o = 0$. Equation 5 was fitted assuming light-limited conditions, because the residual photosynthetic capacity could not otherwise be estimated from the data available in the Lin et al. dataset (Methods S3). Dashed black lines are fitted to all data combined (new model: $y = 0.993 + 0.003$, $r^2_{adj} = 0.87$, $n = 13{,}710$; USO model: $y = 0.981 + 0.009$, $r^2_{adj} = 0.90$, $n = 13{,}734$; both: $p < 10^{-5}$). Thin black lines are 1:1 lines.

Our tests of Equation (3) in comparison to BB and USO highlight several strengths of the physiological approach (Table 2). Firstly, the model can predict stomatal closure under soil drought without the empirical augmentation needed to generate such predictions from BB and USO (Liu et al. 2022; Rogers et al. 2017). Because Equation (3) is based on the now well-established hydroactive response of stomata to leaf water status (Buckley 2005, 2019) (Equation A4), it directly predicts a stomatal response to soil water potential without modifying any fitted parameters; by contrast, BB and USO perform poorly unless their parameters are fitted separately for control and drought conditions (Figure 2). Equation (3) also accommodates hydraulic decline in response to dehydration (decreased K; McCulloh et al. 2019; Sperry and Love 2015), which amplifies stomatal closure—as is often observed (Scoffoni et al. 2023; Zailaa et al. 2025)—and would result in a nonlinear decline in g_{sw} with respect to ψ_s (Figure 1d). The model also predicts, based on broad experimental evidence (Bauer et al. 2013; Buckley 2005, 2019; McAdam and Brodribb 2016), that stomata respond to Δw and soil drought by the same negative feedback mechanism, and this leads to a Δw response with an inverse-hyperbolic shape (Figure 1c). More importantly, it also predicts that the shape of the Δw response is modulated by variation in K (Figure 1c)—a prediction supported by experimental evidence (Choudhary et al. 2014; Detto and Pacala 2022; Hernandez-Santana et al. 2016; Sellin and Kupper 2005; Sinclair et al. 2008; Wedegaertner et al. 2022)—and hence also by anything that affects K, such as hydraulic decline during leaf dehydration (Brodribb and Holbrook 2006; Johnson et al. 2009; Scoffoni and Sack 2017) or changes in temperature (Mills et al. 2026), which affect K via the viscosity of water and possibly by aquaporin function, which influences water transport outside the xylem in leaves and roots (Cochard et al. 2007; Matzner and Comstock 2001; Murai-Hatano et al. 2008; Scoffoni et al. 2023).

These features in turn help Equation (3) to predict and explain the stomatal response to temperature, which has largely been overlooked in formulating previous models. Although temperature affects stomata by increasing Δw, stomata also respond to temperature independently of its effect on Δw (Mills et al. 2024). The response varies but is usually positive (Diao et al. 2024; Mills et al. 2024, 2026; Urban et al. 2017). Since temperature and Δw are strongly but not perfectly correlated in nature (see Figure S2 and figure 6 in Mills et al. 2024), it is essential that models accurately capture the distinct influences of Δw and temperature per se on stomata. Although BB and USO do predict stomatal responses to temperature independent of Δw, their assumption that g_{sw} simply tracks assimilation rate leads to predictions that depend strongly on light and on the parameterization of the photosynthetic temperature response (Figure 7). By contrast, Equation (3) assumes that g_{sw} tracks residual photosynthetic capacity (the difference between the CO_2-saturated value of A [A_m] and A itself; Equation 3b), so the effect of temperature on photosynthetic parameters partially cancels out from Equation (3), making photosynthesis a minor contributor to the temperature response. This eliminates a large influence of light on the temperature response (Figure 7), consistent with observations (Mott and Peak 2010). In Equation (3), the temperature response is mostly driven by effects of temperature on K (Mills et al. 2026; also consistent with observations; Mott and Peak 2010). As knowledge continues to improve about the mechanisms of the temperature response, that knowledge can

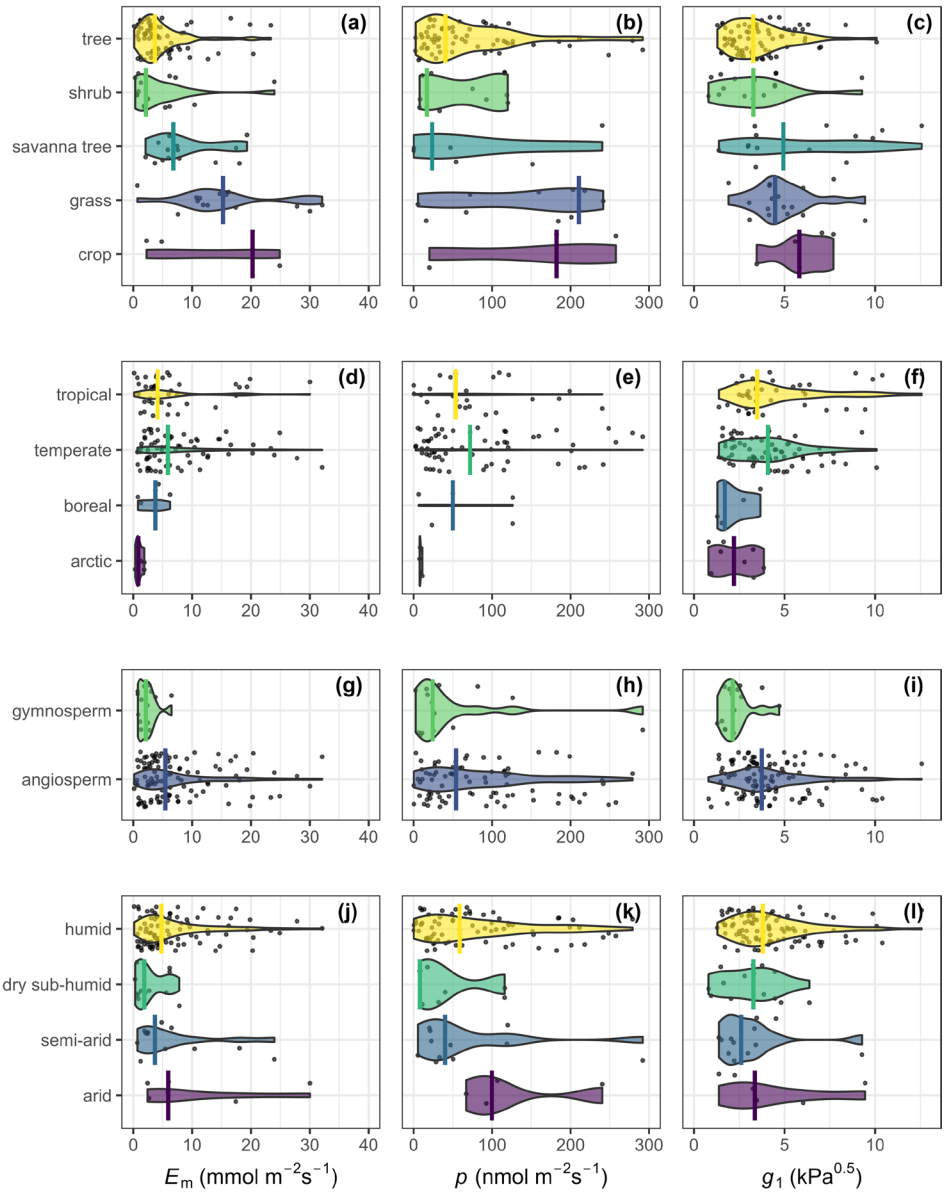

FIGURE 5 | Distributions of parameter values for the new model (in the form given by Equation 5, with parameters E_m and p) and the USO model (with parameter g_1) fitted to data of Lin et al. (2015), within various subgroupings as given by Lin et al.: (a–c) plant functional types ("savanna" refers to "savanna trees" as defined by Lin et al.); (d–f) latitudinal zones (as defined by Lin et al.); (g–i) gymnosperms vs. angiosperms; (j–l) regions of differing aridity. Medians are shown with vertical lines, and are also listed in Table S2, along with numbers of species × site combinations in each category and corresponding median adjusted r^2 values.

be directly incorporated into Equation (3), for example, by incorporating temperature sensitivities for parameters that are confirmed by future experiments to contribute to the temperature response.

The physiological basis of Equation (3) also enables it to correctly predict that nocturnally-open stomata will close in response to soil and atmospheric drought (Barbour and Buckley 2007; Cavender-Bares et al. 2007; Messinger et al. 2006; Mott and Peak 2010), whereas USO and BB incorrectly predict stomatal opening in response to increased Δw at night (e.g., Figure 8). These predictions are important, given current understanding that nocturnal transpiration is a non-trivial fraction of diel totals (Bucci et al. 2004; Buckley et al. 2011; Fisher et al. 2007; Rawson and Clarke 1988; Resco de Dios et al. 2019). The fault in the USO and BB models lies in their prediction of nocturnal opening using a nonzero "intercept" parameter (g_0) that is independent of environmental conditions. This parameter was added to USO to represent the observation of non-zero g_{sw} in darkness—a feature not predicted by CF optimization theory. Lin et al. (2015) later suggested that non-zero g_{sw} in darkness represented cuticular conductance, and proposed setting $g_0 = 0$. However, given that nocturnal conductance responds strongly to factors known to influence stomata, and is often far greater than typical values of cuticular conductance, models of g_{sw} should predict nocturnal stomatal opening, over and above cuticular conductance.

Predictions of the stomatal response to light from the USO and BB models also tend to diverge from observations: whereas USO and BB predict a linear relationship between g_{sw} and the ratio

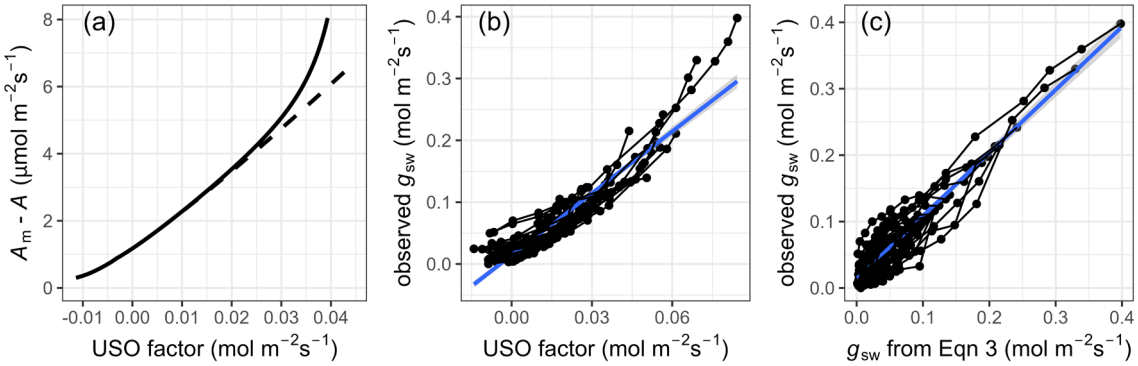

FIGURE 6 | (a) The residual photosynthetic capacity ($A_m - A$) closely tracks the USO factor $\left(1.6A / \left[c_a\sqrt{D}\right]\right)$ under RuBP regeneration-limited conditions (dashed line), but diverges positively from the USO factor under carboxylation-limited conditions (solid line). (b) As a result, at high light and g_{sw}, observed stomatal conductance diverges nonlinearly from the USO factor, and therefore from the USO model's predictions (the blue line is a linear fit to all points, shown to illustrate the nonlinearity between the USO factor and observed g_{sw}). (c) By contrast, because the new model (Equation 3) is based on the residual photosynthetic capacity, its predictions do not similarly diverge from observations. Data from Lamour et al. (2022) [L22; Dataset #4], for responses of g_{sw} to PPFD three tropical tree species. For (c), Equation (3) was applied to environmental and photosynthetic parameters measured by L22, with the parameters ψ_c, s and b_0 fitted separately for each leaf (represented by lines connecting points in [a] and [b]) and K_{25} fixed at 3 mmol m^{-2} s^{-1} MPa^{-1}. We used the curvature parameter and initial slope measured by L22 for assimilation rate to calculate the response of potential electron transport rate (J) to light. For (a), we performed calculations for PPFD between 0 and 1000 μmol m^{-2} s^{-1} (the range used by L22 for most of the data shown in [a, b]), with other parameters set to default values specified in Table 1 (except R_{d25}, which was set to 3 μmol m^{-2} s^{-1} to extend predictions to a similar range of negative values as the data). The dashed line in (a) was extended by setting carboxylation capacity very high to ensure regeneration-limitation at high light, for illustrative purposes.

A/c_a (for a given relative humidity or VPD), nonlinear relationships are often reported, with observed g_{sw} diverging positively from linear predictions at both low light (Ball 1988; Barnard and Bauerle 2013; Duursma et al. 2019) and high light (Kromdijk et al. 2019; Lamour et al. 2022) (Figure 6b). In USO, the divergence at high light reflects that model's assumption that stomata are unaffected by changes in photosynthetic electron transport when photosynthesis is light-saturated, and therefore cannot achieve the theoretical CF optimum in high light (Medlyn et al. 2011); thus, USO predicts lower g_{sw} than CF in high light, and higher g_{sw} than CF in low light (e.g., figure 2 in Buckley et al. 2017). By contrast, Equation (3) assumes that stomata can sense changes in electron transport regardless of what conditions limit photosynthesis, which enables Equation (3) to capture the nonlinear increase in g_{sw} with light (Figure 6c).

Equation (3), unlike BB or USO, also correctly predicts how g_{sw} is affected when the strong coordination typically observed between carboxylation and electron transport capacities (Medlyn et al. 2002; Wullschleger 1993) is broken by mutation or genetic modification. Experiments show that, in high light, antisense suppression of Rubisco activity causes little change in g_{sw}, or even a small increase (von Caemmerer et al. 2004). By contrast, BB and USO predict a large decrease in g_{sw} in such conditions because they assume g_{sw} is directly proportional to A. Equation (3) correctly predicts this effect because, although Rubisco suppression reduces A, it does not affect its CO_2-saturated value (which is determined by electron transport capacity, not carboxylation capacity), so it increases the residual photosynthetic capacity and hence b and g_{sw} (Equation S7). This manifests as a large increase in the value of g_{sw}, and therefore of c_i, predicted by the model, and therefore in the c_i/c_a ratio in plants with suppressed Rubisco activity (Figure 9). By contrast, USO and BB predict a very small increase in c_i/c_a under Rubisco suppression (dashed lines in Figure 9); in fact, if $g_0 = 0$, Rubisco suppression has no effect on c_i/c_a in USO and BB because c_i/c_a is then determined solely by VPD or relative humidity.

The USO model produced better fits (higher adjusted r^2) between modeled and measured conductance than Equation (3) for the dataset of Lin et al. (2015)—only slightly so overall ($r^2 = 0.90$ vs. 0.87) but more so within individual biogeographic regions and plant functional types (median $r^2 = 0.65$ vs. 0.41). Although this would seem to argue against adopting the new model as a predictive tool, we disagree, because the Lin dataset did not include photosynthetic model parameters; as a result, we could not estimate residual photosynthetic capacity to apply the new model without making assumptions that were probably quite inaccurate for many data points. Namely, to estimate b from A and c_i alone, we had to assume that photosynthesis was always regeneration-limited, that respiration was negligible compared to photosynthesis, and that temperature (if not reported) was 25°C (Equation 6). These assumptions would lead to underestimation of the model's performance, but would be unnecessary in real-world applications, because photosynthetic parameters would always be available (as they are when applying USO). Moreover, the new model's novel value lies largely in its ability to natively predict plant responses to soil drought, and to predict and understand variation in those responses in terms of measurable physiological traits like hydraulic conductance and stomatal closure point. The Lin dataset is not suited for illustrating this strength of Equation (3), though the Rodriguez-Dominguez et al. (2016) dataset amply illustrates it (Figure 2).

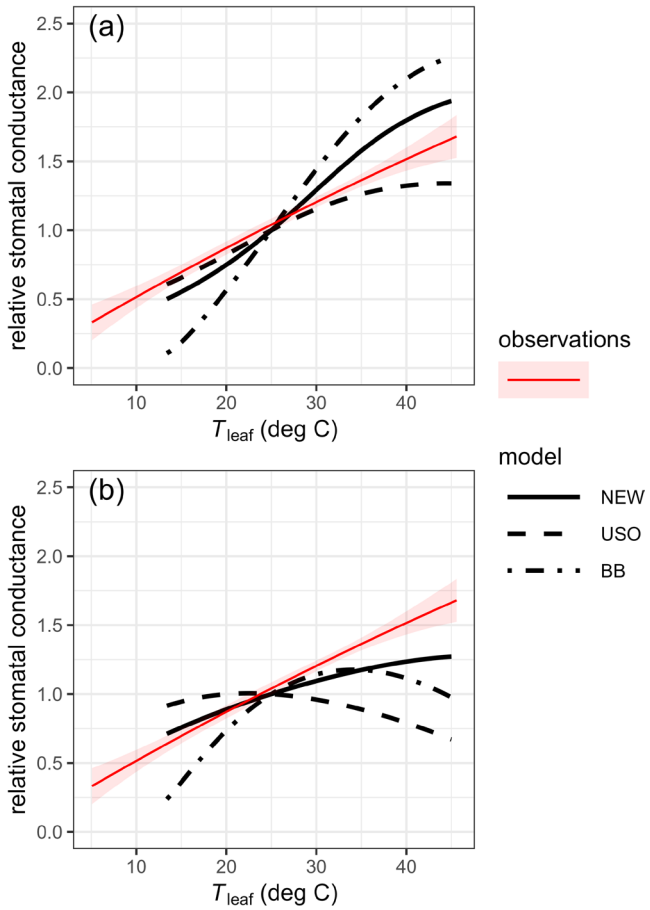

FIGURE 7 | Responses of stomatal conductance to temperature with Δw held constant at 15 mmol mol^{-1}, predicted by Equation (3) ("NEW," solid lines) and by the USO (dashed lines) and Ball-Berry (BB, dash-dot lines) models, under (a) high light (PPFD = 700 μmol m^{-2} s^{-1}) and (b) low light (PPFD = 100 μmol m^{-2} s^{-1}). The thin red lines and shaded areas, which are identical in both panels, represent the mean ± SE of the overall response in published data (at a range of PPFDs, but typically not low values), as compiled by Mills et al. (2024). All responses are expressed relative to the value of stomatal conductance at 25°C.

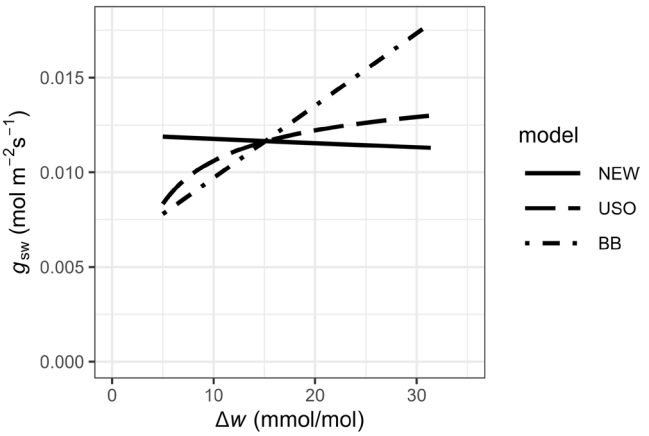

FIGURE 8 | Responses of stomatal conductance to Δw in darkness, predicted by Equation (3) ("NEW") and by the USO and Ball-Berry (BB) models. Equation (3) correctly predicts a negative response, whereas the USO and BB models incorrectly predict positive responses.

4.2 | Effects of CO_2 Enrichment on Stomata

USO, BB and Equation (3) all predict stomatal responses to CO_2. USO and BB achieve this by explicitly including ambient CO_2 (c_a) in the denominator (Equations 1 and 2), whereas Equation (3) predicts the CO_2 response indirectly, via the effect of CO_2 on the residual photosynthetic capacity: as c_i increases, the assimilation rate gets closer to its CO_2-saturated value (A_m), and hence $A_m - A$ decreases. However, Equation (3) also importantly enables prediction of long-term effects of sustained CO_2 enrichment on stomatal conductance. In most leaves, sustained CO_2 enrichment effects are not *responses* of given stomata to changes in CO_2, but rather, they are *differences* in stomatal conductance between leaves, or even whole plants, that developed *de novo* under different levels of CO_2. Those differences in g_{sw} are the collective result of changes in many parameters in response to CO_2 enrichment—changes not only in stomatal apertures, but also in photosynthetic capacity, stomatal density and/or size, and K (Ainsworth and Long 2005; Buckley and Schymanski 2014; Domec et al. 2009; Hao et al. 2018). Indeed, some evidence suggests that differences in g_{sw} under elevated CO_2 are primarily caused by long-term structural acclimation at the whole-plant scale, and minimally by changes in aperture driven by the short-term CO_2 response (Tor-ngern et al. 2015). Thus, models of g_{sw} must be able to assimilate growing understanding of how CO_2 enrichment affects stomata indirectly, via changes in model parameters. This is straightforward for Equation (3) because its parameters have clear biological meaning, but challenging for BB and USO given their parameters' opaque meanings. The USO/BB slope (g_1) is typically conserved under CO_2 enrichment, and this has been interpreted as a lack of acclimation of stomata to CO_2 (Ainsworth and Long 2005; Ainsworth and Rogers 2007; Leakey et al. 2009). More precisely, conservation of g_1 implies lack of acclimation of g_{sw} to changes in *the ratio* A/c_a, not c_a alone. Shifts in A following CO_2 enrichment are accompanied, and partly driven by, declines in photosynthetic capacity (Ainsworth and Long 2005), and like USO/BB, Equation (3) predicts stomatal conductance should track such changes in photosynthetic capacity (Figure 1a). All three models can also accommodate shifts in stomatal density that occur under enrichment (via the parameter g_1 in BB and USO (Dow et al. 2014), and s in Equation 3). However, Equation (3) extends beyond USO and BB by revealing the influence of hydraulic properties on g_{sw}, with the result that—unlike USO and BB—Equation (3) can explicitly accommodate changes in hydraulic conductance caused by elevated CO_2. Species differ widely in the response of hydraulic properties to CO_2 enrichment, and these differences influence how plants respond to soil and atmospheric drought in a high-CO_2 world (Atwell et al. 2007; Domec et al. 2009, 2017; Hao et al. 2018). For example, in *Pinus taeda*, high CO_2 suppressed g_{sw} in moist soils but not under soil drought (Domec et al. 2009). Given growing understanding of the central role of plant hydraulics in plant function and survival, and in ecosystem function more broadly (Anderegg, Konings, et al. 2018; Torres-Ruiz et al. 2024; Wood et al. 2024), it is vital that predictive tools be well structured to accommodate knowledge and mechanistic understanding about hydraulics.

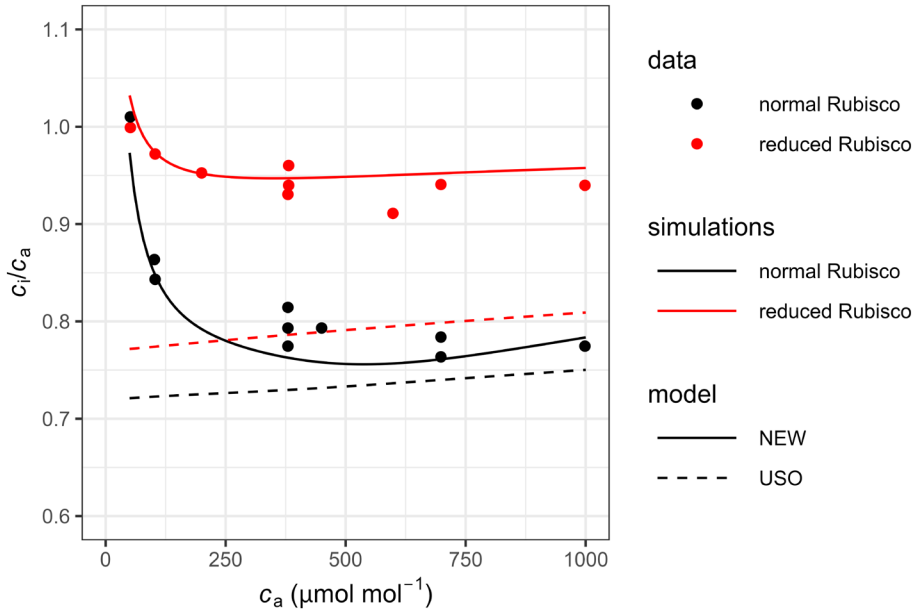

FIGURE 9 | Responses of the ratio of intercellular to ambient CO_2 mole fractions (c_i/c_a) to variation in c_a, observed by von Caemmerer et al. (2004) (symbols) and predicted (lines) either by Equation (3) (solid lines, "NEW") or by the USO model (dashed lines, "USO"), with carboxylation capacity at its default value (50 μmol m^{-2} s^{-1}; "normal Rubisco," black symbols and lines) or reduced by 75% ("reduced Rubisco," red symbols and lines), representing the effects of antisense suppression of Rubisco activity. (Predictions from the Ball-Berry model are identical to those of the USO model in this instance, and thus are not shown.).

4.3 | Parameter Values in the New Model

An essential, yet challenging, aspect of upscaling g_{sw} models is the development of default parameter values based on plant functional type or broader geographic strata (Bonan et al. 2014; Niu et al. 2011). Our exploration of plausible ranges and variability in parameter values (Figure 5) for the proposed model using the Lin et al. (2015) dataset gives a defensible basis for further testing and development. While the Lin dataset does not provide all variables required for complete specification of Equation (3) (soil water potential, stomatal closure point, hydraulic conductance), nor for comparison of its performance with other models, it does provide a robust response space over which parameter distributions can be defined within climatic or taxonomic groups. This approach allowed us to constrain defensible default parameter values for future testing across multiple LSMs to assess model behavior at broader scales.

This exploration of parameter space is also relevant in comparing parameter estimates between the proposed model and the USO model. Our testing of the model (in the form given by Equation 5, with parameters E_m and p) using the dataset of Lin et al. (2015) revealed broadly similar patterns of variation in E_m and p as in the USO parameter, g_1 (Figure 5), across taxa and environments. A general scaling of E_m with g_1 is consistent with the fact that these parameters both determine the g_{sw} obtained for a given photosynthetic capacity (which affects b in the new model and A in the USO model), and for given values of c_a and Δw. Two notable exceptions to this coordination of E_m and g_1 were that E_m was lowest in arctic environments (whereas g_1 was lowest in boreal environments) and highest in arid environments (g_1 was highest in humid environments). Notably, however, there were only 10 species in arid environments, and both E_m and p were exceptionally high in three of them (3–5 orders of magnitude larger than for other species). This likely reflected the fact that Δw varied minimally in the data for those species, making the model's sensitivity to Δw poorly-constrained (Figure S2); setting both E_m and p to large values eliminates the Δw response without affecting the value of g_{sw} at zero Δw (to see this, rearrange Equation 5 as $g_{sw} = [E_m/p]b/[1 + b\Delta w/p]$: large p makes the term involving Δw in the denominator very small, but if E_m is also very large, the numerator is unaffected). Excluding those three sites, the median E_m and p for arid sites were lower than for humid sites (5.2 mmol m^{-2} s^{-1} MPa^{-1} and 41.7 nmol m^{-2} s^{-1}, vs. 6.2 and 73.5, respectively).

It is less obvious why p should scale with g_1, though it seems sensible that it should scale with E_m: since it occurs in a sum with $b\Delta w$ in the denominator of Equation 5, it should roughly scale with b, and the capacities for photosynthesis and water transport (E_m) are known to be coordinated across diverse species and within lineages of closely-related species (Brodribb et al. 2005, 2007; Santiago et al. 2004; Scoffoni et al. 2016). Nevertheless, we found notable exceptions to the scaling of p with E_m. Within non-woody species, p was smallest in crops, whereas E_m and g_1 were both largest in crops. To interpret this, note that the ratio of E_m/p is equivalent to $s(\psi_s - \psi_c)$, so disproportionately higher values of p than of E_m in non-crop grasses and savanna species could indicate larger values of s in crop species, consistent with their generally greater stomatal densities (Bertolino et al. 2019; Haworth et al. 2021); it could also indicate lower soil water potentials (ψ_s) prevailing at the time of measurement for non-crops, consistent with the fact that crops are often heavily irrigated.

5 | Conclusion

We derived a compact, analytical, and tractable model of stomatal conductance, suitable for application in large-scale models of land-atmosphere gas exchange, from an earlier process-based model. The new model contains four physiological parameters, of which all can be fitted empirically if necessary, but two are straightforward to measure experimentally (namely, soil-leaf hydraulic conductance and the stomatal closure point). Due to its origin in a mechanistic model based on the hydroactive feedback mechanism of stomatal responses to soil and atmospheric drought, the new model natively predicts stomatal closure in response to declining soil water potential. The model also overcomes several drawbacks of empirical models, including divergence of those models from observations in low and high light, and their incorrect predictions about how drought affects nocturnal stomatal conductance, how temperature affects stomata independent of evaporative demand, and how independent variation in carboxylation and electron transport capacities affects stomata. By providing a tractable tool for predicting gas exchange with a mathematical structure that is transparently based on physiological understanding, the new model offers the prospect of more confident predictions than possible with empirical models when applied beyond the parameterization domain—such as in future climate scenarios. Given the strong dependence, highlighted by this process framework, of stomatal conductance on hydraulic parameters including soil water potential, soil–plant hydraulic conductance, and the stomatal closure point, we recommend that these latter parameters be measured concurrently with stomatal conductance when feasible.

Author Contributions

Thomas N. Buckley: conceptualization, investigation, funding acquisition, writing – original draft, methodology, validation, visualization, writing – review and editing, software, formal analysis, project administration, data curation, supervision, resources. **Julien Lamour:** writing – original draft, methodology, validation, visualization, writing – review and editing, software. **David M. Barnard:** writing – review and editing, visualization, writing – original draft. **Daniel W. Buckley:** writing – review and editing, validation, methodology, formal analysis. **Andrew J. Jarvis:** conceptualization, writing – review and editing, methodology, formal analysis. **Antonio Diaz-Espejo:** writing – review and editing, validation, methodology, conceptualization. **Alistair Rogers:** writing – original draft, writing – review and editing, visualization, validation, methodology. **Lawren Sack:** writing – original draft, writing – review and editing, conceptualization, methodology.

Acknowledgments

T.N.B. acknowledges support from the National Science Foundation (Award #2307341) and the National Institute of Food and Agriculture (Hatch grant #CA-D-PLS-2790-H). A.R. was supported by the Next Generation Ecosystem Experiments-Tropics project funded by the US Department of Energy, Office of Science, Office of Biological and Environmental Research and by U.S. Department of Energy Contract No. DE-AC02-05CH11231 to Lawrence Berkeley National Laboratory.

Funding

This work was supported by the National Science Foundation (2307341), National Institute of Food and Agriculture (Hatch grant #CA-D-PLS-2790-H), and U.S. Department of Energy (DE-AC02-05CH11231, Next Generation Ecosystem Experiments-Tropics).

Conflicts of Interest

The authors declare no conflicts of interest.

Data Availability Statement

R code used to generate all figures, and data for Datasets #1 and #4, are provided in a GitHub repository at https://doi.org/10.5281/zenodo.21105704. Data for Datasets #2 and #3 are available at repositories previously created by the original authors of those datasets: https://figshare.com/articles/dataset/Optimal_stomatal_behaviour_around_the_world/1304289?file=1886204 and https://doi.org/10.15486/ngt/1781004, respectively.

References

Ainsworth, E. A., and S. P. Long. 2005. "What Have We Learned From 15 Years of Free-Air CO_2 Enrichment (FACE)? A Meta-Analytic Review of the Responses of Photosynthesis, Canopy Properties and Plant Production to Rising CO_2." *New Phytologist* 165: 351–372.

Ainsworth, E. A., and A. Rogers. 2007. "The Response of Photosynthesis and Stomatal Conductance to Rising $[CO_2]$: Mechanisms and Environmental Interactions." *Plant, Cell & Environment* 30: 258–270.

Anderegg, W. R., A. G. Konings, A. T. Trugman, et al. 2018. "Hydraulic Diversity of Forests Regulates Ecosystem Resilience During Drought." *Nature* 561, no. 7724: 538–541.

Anderegg, W. R., A. Wolf, A. Arango-Velez, et al. 2018. "Woody Plants Optimise Stomatal Behaviour Relative to Hydraulic Risk." *Ecology Letters* 21, no. 7: 968–977.

Aphalo, P., and P. Jarvis. 1993. "An Analysis of Ball's Empirical Model of Stomatal Conductance." *Annals of Botany* 72, no. 4: 321–327.

Atwell, B. J., M. L. Henery, G. S. Rogers, S. P. Seneweera, M. Treadwell, and J. P. Conroy. 2007. "Canopy Development and Hydraulic Function in *Eucalyptus tereticornis* Grown in Drought in CO_2-Enriched Atmospheres." *Functional Plant Biology* 34, no. 12: 1137–1149.

Ball, J. T. 1988. *An Analysis of Stomatal Conductance*. Stanford University.

Ball, J. T., I. E. Woodrow, and J. A. Berry. 1987. "A Model Predicting Stomatal Conductance and Its Contribution to the Control of Photosynthesis Under Different Environmental Conditions." In *Progress in Photosynthesis Research*, edited by J. Biggens, 221–224. Martinus Nijhoff Publishers.

Barbour, M. M., and T. N. Buckley. 2007. "The Stomatal Response to Evaporative Demand Persists at Night in *Ricinus communis* Plants With High Nocturnal Conductance." *Plant, Cell & Environment* 30: 711–721.

Barnard, D., and W. Bauerle. 2013. "The Implications of Minimum Stomatal Conductance on Modeling Water Flux in Forest Canopies." *Journal of Geophysical Research: Biogeosciences* 118, no. 3: 1322–1333.

Bartlett, M. K., C. Scoffoni, R. Ardy, et al. 2012. "Rapid Determination of Comparative Drought Tolerance Traits: Using an Osmometer to Predict Turgor Loss Point." *Methods in Ecology and Evolution* 3, no. 5: 880–888. https://doi.org/10.1111/j.2041-210X.2012.00230.x.

Bartlett, M. K., C. Scoffoni, and L. Sack. 2012. "The Determinants of Leaf Turgor Loss Point and Prediction of Drought Tolerance of Species and Biomes: A Global Meta-Analysis." *Ecology Letters* 15, no. 5: 393–405. https://doi.org/10.1111/j.1461-0248.2012.01751.x.

Bartlett, M. K., Y. Zhang, N. Kreidler, et al. 2014. "Global Analysis of Plasticity in Turgor Loss Point, a Key Drought Tolerance Trait." *Ecology Letters* 17, no. 12: 1580–1590.

Bauer, H., P. Ache, S. Lautner, et al. 2013. "The Stomatal Response to Reduced Relative Humidity Requires Guard Cell-Autonomous ABA Synthesis." *Current Biology* 23, no. 1: 53–57.

Bernacchi, C., C. Pimentel, and S. P. Long. 2003. "In Vivo Temperature Response Functions of Parameters Required to Model RuBP-Limited Photosynthesis." *Plant, Cell & Environment* 26, no. 9: 1419–1430.

Bernacchi, C. J., E. L. Singsaas, C. Pimentel, A. R. J. Portis, and S. P. Long. 2001. "Improved Temperature Response Functions for Models of Rubisco-Limited Photosynthesis." *Plant, Cell and Environment* 24: 253–259.

Berry, J. A., D. J. Beerling, and P. J. Franks. 2010. "Stomata: Key Players in the Earth System, Past and Present." *Current Opinion in Plant Biology* 13, no. 3: 232–239. https://doi.org/10.1016/j.pbi.2010.04.013.

Bertolino, L. T., R. S. Caine, and J. E. Gray. 2019. "Impact of Stomatal Density and Morphology on Water-Use Efficiency in a Changing World." *Frontiers in Plant Science* 10: 225.

Bonan, G., M. Williams, R. Fisher, and K. Oleson. 2014. "Modeling Stomatal Conductance in the Earth System: Linking Leaf Water-Use Efficiency and Water Transport Along the Soil–Plant–Atmosphere Continuum." *Geoscientific Model Development* 7, no. 5: 2193–2222.

Brett, M. T. 2004. "When Is a Correlation Between Non-Independent Variables "Spurious"?" *Oikos* 105, no. 3: 647–656.

Brodribb, T. J., and T. S. Feild. 2000. "Stem Hydraulic Supply Is Linked to Leaf Photosynthetic Capacity: Evidence From New Caledonian and Tasmanian Rainforests." *Plant, Cell & Environment* 23: 1381–1388.

Brodribb, T. J., T. S. Feild, and G. J. Jordan. 2007. "Leaf Maximum Photosynthetic Rate and Venation Are Linked by Hydraulics." *Plant Physiology* 144, no. 4: 1890–1898.

Brodribb, T. J., and N. M. Holbrook. 2006. "Declining Hydraulic Efficiency as Transpiring Leaves Desiccate: Two Types of Response." *Plant, Cell and Environment* 29, no. 12: 2205–2215. https://doi.org/10.1111/j.1365-3040.2006.01594.x.

Brodribb, T. J., N. M. Holbrook, and M. V. Gutierrez. 2002. "Hydraulic and Photosynthetic Coordination in Seasonally Dry Tropical Forest Trees." *Plant, Cell & Environment* 25: 1435–1444.

Brodribb, T. J., N. M. Holbrook, M. A. Zwieniecki, and B. Palma. 2005. "Leaf Hydraulic Capacity in Ferns, Conifers and Angiosperms: Impacts on Photosynthetic Maxima." *New Phytologist* 165, no. 3: 839–846. https://doi.org/10.1111/j.1469-8137.2004.01259.x.

Bucci, S. J., F. G. Scholz, G. Goldstein, et al. 2004. "Processes Preventing Nocturnal Equilibration Between Leaf and Soil Water Potential in Tropical Savanna Woody Species." *Tree Physiology* 24: 1119–1127.

Buckley, T. N. 2005. "The Control of Stomata by Water Balance (Tansley Review)." *New Phytologist* 168: 275–292.

Buckley, T. N. 2019. "How Do Stomata Respond to Water Status?" *New Phytologist* 224: 21–36.

Buckley, T. N., E. H. Frehner, and B. N. Bailey. 2023. "Kinetic Factors of Physiology and the Dynamic Light Environment Influence the Economic Landscape of Short-Term Hydraulic Risk." *New Phytologist* 238, no. 2: 529–548.

Buckley, T. N., K. A. Mott, and G. D. Farquhar. 2003. "A Hydromechanical and Biochemical Model of Stomatal Conductance." *Plant, Cell and Environment* 26, no. 10: 1767–1785.

Buckley, T. N., L. Sack, and G. D. Farquhar. 2017. "Optimal Plant Water Economy." *Plant, Cell & Environment* 40, no. 6: 881–896.

Buckley, T. N., and S. J. Schymanski. 2014. "Stomatal Optimisation in Relation to Atmospheric CO_2." *New Phytologist* 201, no. 2: 372–377.

Buckley, T. N., T. L. Turnbull, and M. A. Adams. 2012. "Simple Models for Stomatal Conductance Derived From a Process Model: Cross-Validation Against Sap Flux Data." *Plant, Cell & Environment* 35, no. 9: 1647–1662. https://doi.org/10.1111/j.1365-3040.2012.02515.x.

Buckley, T. N., T. L. Turnbull, S. Pfautsch, and M. A. Adams. 2011. "Nocturnal Water Loss in Mature Subalpine *Eucalyptus delegatensis* Tall Open Forests and Adjacent *E. pauciflora* Woodlands." *Ecology and Evolution* 1, no. 3: 435–450. https://doi.org/10.1002/ece3.44.

Busch, F. A. 2014. "Opinion: The Red-Light Response of Stomatal Movement Is Sensed by the Redox State of the Photosynthetic Electron Transport Chain." *Photosynthesis Research* 119: 131–140. https://doi.org/10.1007/s11120-013-9805-6.

Caemmerer, S., and G. D. Farquhar. 1981. "Some Relationships Between the Biochemistry of Photosynthesis and the Gas Exchange of Leaves." *Planta* 153, no. 4: 376–387. https://doi.org/10.1007/bf00384257.

Caird, M. A., J. H. Richards, and L. A. Donovan. 2007. "Nighttime Stomatal Conductance and Transpiration in C3 and C4 Plants." *Plant Physiology* 143: 4–10.

Cavender-Bares, J., L. Sack, and J. Savage. 2007. "Atmospheric and Soil Drought Reduce Nocturnal Conductance in Live Oaks." *Tree Physiology* 27: 611–620.

Choat, B., T. J. Brodribb, C. R. Brodersen, R. A. Duursma, R. López, and B. E. Medlyn. 2018. "Triggers of Tree Mortality Under Drought." *Nature* 558, no. 7711: 531–539.

Choudhary, S., T. R. Sinclair, C. D. Messina, and M. Cooper. 2014. "Hydraulic Conductance of Maize Hybrids Differing in Transpiration Response to Vapor Pressure Deficit." *Crop Science* 54, no. 3: 1147–1152.

Cochard, H., J. S. Venisse, T. S. Barigah, et al. 2007. "Putative Role of Aquaporins in Variable Hydraulic Conductance of Leaves in Response to Light." *Plant Physiology* 143, no. 1: 122–133. https://doi.org/10.1104/pp.106.090092.

Collatz, G. J., M. Ribas-Carbo, and J. A. Berry. 1992. "Coupled Photosynthesis-Stomatal Conductance Model for Leaves of C4 Plants." *Functional Plant Biology* 19, no. 5: 519–538.

Comstock, J., and M. Mencuccini. 1998. "Control of Stomatal Conductance by Leaf Water Potential in *Hymenoclea salsola* (T & G), a Desert Subshrub." *Plant, Cell and Environment* 21, no. 10: 1029–1038.

Cowan, I. R., and G. D. Farquhar. 1977. "Stomatal Function in Relation to Leaf Metabolism and Environment." *Symposium of the Society for Experimental Biology* 31: 471–505.

De Kauwe, M. G., J. Kala, Y.-S. Lin, et al. 2015. "A Test of an Optimal Stomatal Conductance Scheme Within the CABLE Land Surface Model." *Geoscientific Model Development* 8, no. 2: 431–452.

de Pury, D. G. G., and G. D. Farquhar. 1997. "Simple Scaling of Photosynthesis From Leaves to Canopies Without the Errors of Big-Leaf Models." *Plant, Cell and Environment* 20: 537–557.

Deans, R. M., T. J. Brodribb, F. A. Busch, and G. D. Farquhar. 2020. "Optimization Can Provide the Fundamental Link Between Leaf Photosynthesis, Gas Exchange and Water Relations." *Nature Plants* 6, no. 9: 1116–1125.

Delwiche, M. J., and J. R. Cooke. 1977. "An Analytical Model of the Hydraulic Aspects of Stomatal Function." *Journal of Theoretical Biology* 69: 131–141.

Delzon, S., and H. Cochard. 2014. "Recent Advances in Tree Hydraulics Highlight the Ecological Significance of the Hydraulic Safety Margin." *New Phytologist* 203, no. 2: 355–358. https://doi.org/10.1111/nph.12798.

DeMichele, D. W., and P. J. H. Sharpe. 1973. "An Analysis of the Mechanics of Guard Cell Motion." *Journal of Theoretical Biology* 41: 77–96.

Detto, M., and S. W. Pacala. 2022. "Plant Hydraulics, Stomatal Control, and the Response of a Tropical Forest to Water Stress Over Multiple Temporal Scales." *Global Change Biology* 28, no. 14: 4359–4376.

Dewar, R., T. Hölttä, and Y. Salmon. 2022. "Exploring Optimal Stomatal Control Under Alternative Hypotheses for the Regulation of Plant Sources and Sinks." *New Phytologist* 233, no. 2: 639–654.

Dewar, R. C. 1995. "Interpretation of an Empirical Model for Stomatal Conductance in Terms of Guard Cell Function." *Plant, Cell and Environment* 18: 365–372.

Dewar, R. C. 2002. "The Ball-Berry-Leuning and Tardieu-Davies Stomatal Models: Synthesis and Extension Within a Spatially Aggregated Picture of Guard Cell Function." *Plant, Cell and Environment* 25: 1383–1398.

Diao, H., L. A. Cernusak, M. Saurer, A. Gessler, R. T. W. Siegwolf, and M. M. Lehmann. 2024. "Uncoupling of Stomatal Conductance and Photosynthesis at High Temperatures: Mechanistic Insights From Online Stable Isotope Techniques." *New Phytologist* 241, no. 6: 2366–2378. https://doi.org/10.1111/nph.19558.

Domec, J.-C., S. Palmroth, E. Ward, C. A. Maier, M. ThÉRÉZien, and R. A. M. Oren. 2009. "Acclimation of Leaf Hydraulic Conductance and Stomatal Conductance of *Pinus taeda* (Loblolly Pine) to Long-Term Growth in Elevated CO_2 (Free-Air CO_2 Enrichment) and N-Fertilization." *Plant, Cell & Environment* 32, no. 11: 1500–1512. https://doi.org/10.1111/j.1365-3040.2009.02014.x.

Domec, J.-C., D. D. Smith, and K. A. McCulloh. 2017. "A Synthesis of the Effects of Atmospheric Carbon Dioxide Enrichment on Plant Hydraulics: Implications for Whole-Plant Water Use Efficiency and Resistance to Drought." *Plant, Cell & Environment* 40, no. 6: 921–937.

Domingues, T. F., L. A. Martinelli, and J. R. Ehleringer. 2014. "Seasonal Patterns of Leaf-Level Photosynthetic Gas Exchange in an Eastern Amazonian Rain Forest." *Plant Ecology and Diversity* 7, no. 1–2: 189–203.

Dow, G. J., D. C. Bergmann, and J. A. Berry. 2014. "An Integrated Model of Stomatal Development and Leaf Physiology." *New Phytologist* 201, no. 4: 1218–1226.

Drake, J. E., M. G. Tjoelker, A. Vårhammar, et al. 2018. "Trees Tolerate an Extreme Heatwave via Sustained Transpirational Cooling and Increased Leaf Thermal Tolerance." *Global Change Biology* 24, no. 6: 2390–2402.

Dukes, J. S., C. Xu, C. Liao, et al. 2026. "Improving the Representation of Plant Water Stress and Water Use in Earth System Models." *New Phytologist* 249: 39–55.

Duursma, R. A., C. J. Blackman, R. Lopéz, N. K. Martin-StPaul, H. Cochard, and B. E. Medlyn. 2019. "On the Minimum Leaf Conductance: Its Role in Models of Plant Water Use, and Ecological and Environmental Controls." *New Phytologist* 221, no. 2: 693–705.

Edwards, M., H. Meidner, and D. W. Sheriff. 1976. "Direct Measurements of Turgor Pressure Potentials of Guard Cells. II. The Mechanical Advantage of Subsidiary Cells, the Spannungsphase, and the Optimum Leaf Water Deficit." *Journal of Experimental Botany* 96: 163–171.

Eller, C. B., L. Rowland, M. Mencuccini, et al. 2020. "Stomatal Optimization Based on Xylem Hydraulics (SOX) Improves Land Surface Model Simulation of Vegetation Responses to Climate." *New Phytologist* 226, no. 6: 1622–1637. https://doi.org/10.1111/nph.16419.

Eller, C. B., L. Rowland, R. S. Oliveira, et al. 2018. "Modelling Tropical Forest Responses to Drought and El Niño With a Stomatal Optimization Model Based on Xylem Hydraulics." *Philosophical Transactions of the Royal Society, B: Biological Sciences* 373, no. 1760: 20170315.

Farquhar, G. D., S. von Caemmerer, and J. A. Berry. 1980. "A Biochemical Model of Photosynthetic CO_2 Assimilation in Leaves of C3 Species." *Planta* 149: 78–90.

Farquhar, G. D., and S. C. Wong. 1984. "An Empirical Model of Stomatal Conductance." *Australian Journal of Plant Physiology* 11: 191–210.

Fisher, J. B., D. D. Baldocchi, L. Misson, T. E. Dawson, and A. H. Goldstein. 2007. "What the Towers Don't See at Night: Nocturnal Sap Flow in Trees and Shrubs at Two AmeriFlux Sites in California." *Tree Physiology* 27: 597–610.

Forster, M. A. 2014. "How Significant Is Nocturnal Sap Flow?" *Tree Physiology* 34, no. 7: 757–765.

Franks, P. J., J. A. Berry, D. L. Lombardozzi, and G. B. Bonan. 2017. "Stomatal Function Across Temporal and Spatial Scales: Deep-Time Trends, Land-Atmosphere Coupling and Global Models." *Plant Physiology* 174, no. 2: 583–602.

Franks, P. J., G. B. Bonan, J. A. Berry, et al. 2018. "Comparing Optimal and Empirical Stomatal Conductance Models for Application in Earth System Models." *Global Change Biology* 24, no. 12: 5708–5723.

Franks, P. J., I. R. Cowan, and G. D. Farquhar. 1998. "A Study of Stomatal Mechanics Using the Cell Pressure Probe." *Plant, Cell and Environment* 21: 94–100.

Fricke, W. 2019. "Night-Time Transpiration–Favouring Growth?" *Trends in Plant Science* 24, no. 4: 311–317.

Hao, G.-Y., N. M. Holbrook, M. A. Zwieniecki, V. P. Gutschick, and H. BassiriRad. 2018. "Coordinated Responses of Plant Hydraulic Architecture With the Reduction of Stomatal Conductance Under Elevated CO_2 Concentration." *Tree Physiology* 38, no. 7: 1041–1052.

Haworth, M., G. Marino, F. Loreto, and M. Centritto. 2021. "Integrating Stomatal Physiology and Morphology: Evolution of Stomatal Control and Development of Future Crops." *Oecologia* 197, no. 4: 867–883.

Hernandez-Santana, V., C. M. Rodriguez-Dominguez, J. E. Fernández, and A. Diaz-Espejo. 2016. "Role of Leaf Hydraulic Conductance in the Regulation of Stomatal Conductance in Almond and Olive in Response to Water Stress." *Tree Physiology* 36, no. 6: 725–735.

Hetherington, A. M., and F. I. Woodward. 2003. "The Role of Stomata in Sensing and Driving Environmental Change." *Nature* 424: 901–908.

Hills, A., Z.-H. Chen, A. Amtmann, M. R. Blatt, and V. Lew. 2012. "OnGuard—A Computational Platform for Quantitative Kinetic Modelling of Guard Cell Physiology." *Plant Physiology* 159: 1026–1042.

Jarvis, A. J., and W. J. Davies. 1998. "The Coupled Response of Stomatal Conductance to Photosynthesis and Transpiration." *Journal of Experimental Botany* 49: 399–406.

Johnson, D. M., D. R. Woodruff, K. A. McCulloh, and F. C. Meinzer. 2009. "Leaf Hydraulic Conductance, Measured In Situ, Declines and Recovers Daily: Leaf Hydraulics, Water Potential and Stomatal Conductance in Four Temperate and Three Tropical Tree Species." *Tree Physiology* 29, no. 7: 879–887.

Jones, H. 1985. "Partitioning Stomatal and Non-Stomatal Limitations to Photosynthesis." *Plant, Cell and Environment* 8, no. 2: 95–104.

Kavanagh, K. L., R. Pangle, and A. D. Schotzko. 2007. "Nocturnal Transpiration Causing Disequilibrium Between Soil and Stem Predawn Water Potential in Mixed Conifer Forests of Idaho." *Tree Physiology* 27: 621–629.

Kennedy, D., S. Swenson, K. W. Oleson, et al. 2019. "Implementing Plant Hydraulics in the Community Land Model, Version 5." *Journal of Advances in Modeling Earth Systems* 11, no. 2: 485–513.

Kromdijk, J., K. Głowacka, and S. P. Long. 2019. "Predicting Light-Induced Stomatal Movements Based on the Redox State of Plastoquinone: Theory and Validation." *Photosynthesis Research* 141, no. 1: 83–97.

Kuromori, T., E. Sugimoto, and K. Shinozaki. 2014. "Inter-Tissue Signal Transfer of Abscisic Acid From Vascular Cells to Guard Cells." *Plant Physiology* 164: 1587–1592.

Lamour, J., K. J. Davidson, K. S. Ely, et al. 2022. "An Improved Representation of the Relationship Between Photosynthesis and

Stomatal Conductance Leads to More Stable Estimation of Conductance Parameters and Improves the Goodness-Of-Fit Across Diverse Data Sets." *Global Change Biology* 28, no. 11: 3537–3556.

Lamour, J., D. C. Souza, B. O. Gimenez, et al. 2023. "Wood-Density Has no Effect on Stomatal Control of Leaf-Level Water Use Efficiency in an Amazonian Forest." *Plant, Cell & Environment* 46, no. 12: 3806–3821.

Lawson, T. 2009. "Guard Cell Photosynthesis and Stomatal Function." *New Phytologist* 181, no. 1: 13–34.

Lawson, T., and J. Matthews. 2020. "Guard Cell Metabolism and Stomatal Function." *Annual Review of Plant Biology* 71: 273–302.

Lawson, T., I. Terashima, T. Fujita, and Y. Wang. 2018. "Coordination Between Photosynthesis and Stomatal Behavior." In *The Leaf: A Platform for Performing Photosynthesis*, edited by I. T. W. W. Adams III, 141–162. Springer.

Leakey, A. D. B., E. A. Ainsworth, C. J. Bernacchi, A. Rogers, S. P. Long, and D. R. Ort. 2009. "Elevated CO_2 Effects on Plant Carbon, Nitrogen, and Water Relations: Six Important Lessons From FACE." *Journal of Experimental Botany* 60, no. 10: 2859–2876. https://doi.org/10.1093/jxb/erp096.

Leuning, R., F. M. Kelliher, D. G. G. de Pury, and E. D. Schulze. 1995. "Leaf Nitrogen, Photosynthesis, Conductance and Transpiration: Scaling From Leaves to Canopies." *Plant, Cell and Environment* 18: 1183–1200.

Li, L., Z. Yang, A. M. Matheny, et al. 2021. "Representation of Plant Hydraulics in the Noah-MP Land Surface Model: Model Development and Multiscale Evaluation." *Journal of Advances in Modeling Earth Systems* 13, no. 4: e2020MS002214.

Li, Q., S. P. Serbin, J. Lamour, K. J. Davidson, K. S. Ely, and A. Rogers. 2022. "Implementation and Evaluation of the Unified Stomatal Optimization Approach in the Functionally Assembled Terrestrial Ecosystem Simulator (FATES)." *Geoscientific Model Development* 15, no. 11: 4313–4329.

Lin, Y.-S., B. E. Medlyn, R. A. Duursma, et al. 2015. "Optimal Stomatal Behaviour Around the World." *Nature Climate Change* 5, no. 5: 459–464.

Liu, C., L. Sack, Y. Li, et al. 2023. "Relationships of Stomatal Morphology to the Environment Across Plant Communities." *Nature Communications* 14, no. 1: 6629.

Liu, M., H. Wang, X. Liu, et al. 2022. "Integration of Carbon Dioxide Concentration in a Simplified Process-Based Model for Evapotranspiration Estimation in an Old-Growth Forest." *Forest Ecology and Management* 520: 120392. https://doi.org/10.1016/j.foreco.2022.120392.

Liu, N., T. N. Buckley, X. He, et al. 2019. "Improvement of a Simplified Process-Based Model for Estimating Transpiration Under Water-Limited Conditions." *Hydrological Processes* 33, no. 12: 1670–1685.

Liu, N., H. Wang, X. He, et al. 2019. "A Hybrid Transpiration Model for Water-Limited Conditions." *Journal of Hydrology* 578: 124104.

Lloyd, J., K. Bloomfield, T. F. Domingues, and G. D. Farquhar. 2013. "Photosynthetically Relevant Foliar Traits Correlating Better on a Mass vs an Area Basis: Of Ecophysiological Relevance or Just a Case of Mathematical Imperatives and Statistical Quicksand?" *New Phytologist* 199, no. 2: 311–321.

Lombardozzi, D. L., M. J. Zeppel, R. A. Fisher, and A. Tawfik. 2017. "Representing Nighttime and Minimum Conductance in CLM4. 5: Global Hydrology and Carbon Sensitivity Analysis Using Observational Constraints." *Geoscientific Model Development* 10, no. 1: 321–331.

Maréchaux, I., M. K. Bartlett, L. Sack, et al. 2015. "Drought Tolerance as Predicted by Leaf Water Potential at Turgor Loss Point Varies Strongly Across Species Within an Amazonian Forest." *Functional Ecology* 29, no. 10: 1268–1277.

Matzner, S., and J. Comstock. 2001. "The Temperature Dependence of Shoot Hydraulic Resistance: Implications for Stomatal Behaviour and Hydraulic Limitation." *Plant, Cell & Environment* 24, no. 12: 1299–1307.

McAdam, S., and T. Brodribb. 2018. "Mesophyll Cells Are the Main Site of Abscisic Acid Biosynthesis in Water-Stressed Leaves." *Plant Physiology* 177: 911–917.

McAdam, S. A., and T. J. Brodribb. 2016. "Linking Turgor With ABA Biosynthesis: Implications for Stomatal Responses to Vapour Pressure Deficit Across Land Plants." *Plant Physiology* 171: 2008–2016.

McCulloh, K. A., J.-C. Domec, D. M. Johnson, D. D. Smith, and F. C. Meinzer. 2019. "A Dynamic Yet Vulnerable Pipeline: Integration and Coordination of Hydraulic Traits Across Whole Plants." *Plant, Cell and Environment* 42, no. 10: 2789–2807. https://doi.org/10.1111/pce.13607.

Medlyn, B. E., E. Dreyer, D. Ellsworth, et al. 2002. "Temperature Response of Parameters of a Biochemically Based Model of Photosynthesis. II. A Review of Experimental Data." *Plant, Cell & Environment* 25, no. 9: 1167–1179. https://doi.org/10.1046/j.1365-3040.2002.00891.x.

Medlyn, B. E., R. A. Duursma, D. Eamus, et al. 2011. "Reconciling the Optimal and Empirical Approaches to Modelling Stomatal Conductance." *Global Change Biology* 17, no. 6: 2134–2144. https://doi.org/10.1111/j.1365-2486.2010.02375.x.

Mencuccini, M. 2003. "The Ecological Significance of Long-Distance Water Transport: Short-Term Regulation, Long-Term Acclimation and the Hydraulic Costs of Stature Across Plant Life Forms." *Plant, Cell and Environment* 26: 163–182.

Messinger, S. M., T. N. Buckley, and K. A. Mott. 2006. "Evidence for Involvement of Photosynthetic Processes in the Stomatal Response to CO_2." *Plant Physiology* 140: 771–778.

Mills, C., M. K. Bartlett, and T. N. Buckley. 2024. "The Poorly-Explored Stomatal Response to Temperature at Constant Evaporative Demand." *Plant, Cell & Environment* 47, no. 9: 3428–3446.

Mills, C., M. K. Bartlett, and T. N. Buckley. 2026. "The Stomatal Response to Temperature Is Enhanced by High Evaporative Demand, Consistent With a Partially Hydraulic Mechanism." *Plant, Cell and Environment* 49: 1958–1968. https://doi.org/10.1111/pce.70347.

Mott, K. A. 2009. "Opinion: Stomatal Responses to Light and CO_2 Depend on the Mesophyll." *Plant, Cell & Environment* 32, no. 11: 1479–1486. https://doi.org/10.1111/j.1365-3040.2009.02022.x.

Mott, K. A., and D. Peak. 2010. "Stomatal Responses to Humidity and Temperature in Darkness." *Plant, Cell & Environment* 33, no. 7: 1084–1090.

Murai-Hatano, M., T. Kuwagata, J. Sakurai, et al. 2008. "Effect of Low Root Temperature on Hydraulic Conductivity of Rice Plants and the Possible Role of Aquaporins." *Plant and Cell Physiology* 49, no. 9: 1294–1305.

Niu, G., Z. Yang, K. E. Mitchell, et al. 2011. "The Community Noah Land Surface Model With Multiparameterization Options (Noah-MP): 1. Model Description and Evaluation With Local-Scale Measurements." *Journal of Geophysical Research: Atmospheres* 116: D12109.

Novick, K. A., D. L. Ficklin, D. Baldocchi, et al. 2022. "Confronting the Water Potential Information Gap." *Nature Geoscience* 15, no. 3: 158–164.

Oren, R., J. S. Sperry, G. G. Katul, et al. 1999. "Survey and Synthesis of Intra- and Interspecific Variation in Stomatal Sensitivity to Vapour Pressure Deficit." *Plant, Cell and Environment* 22: 1515–1526.

Phillips, N., B. J. Bond, N. G. McDowell, and M. G. Ryan. 2002. "Canopy and Hydraulic Conductance in Young, Mature and Old Douglas-Fir Trees." *Tree Physiology* 22: 205–211.

Poyatos, R., V. Granda, V. Flo, et al. 2020. "Global Transpiration Data From Sap Flow Measurements: The SAPFLUXNET Database." *Earth System Science Data Discussions* 2020: 1–57.

Prentice, I. C., N. Dong, S. M. Gleason, V. Maire, and I. J. Wright. 2014. "Balancing the Costs of Carbon Gain and Water Transport: Testing a New Theoretical Framework for Plant Functional Ecology." *Ecology Letters* 17, no. 1: 82–91.

Rawson, H. M., and J. M. Clarke. 1988. "Nocturnal Transpiration in Wheat." *Australian Journal of Plant Physiology* 15: 397–406.

Resco de Dios, V., F. I. Chowdhury, E. Granda, Y. Yao, and D. T. Tissue. 2019. "Assessing the Potential Functions of Nocturnal Stomatal Conductance in C3 and C4 Plants." *New Phytologist* 223, no. 4: 1696–1706.

Rodriguez-Dominguez, C. M., T. N. Buckley, G. Egea, et al. 2016. "Most Stomatal Closure in Woody Species Under Moderate Drought Can Be Explained by Stomatal Responses to Leaf Turgor." *Plant, Cell & Environment* 39, no. 9: 2014–2026.

Rogers, A., B. E. Medlyn, J. S. Dukes, et al. 2017. "A Roadmap for Improving the Representation of Photosynthesis in Earth System Models." *New Phytologist* 213, no. 1: 22–42.

Sabot, M. E., M. G. De Kauwe, A. J. Pitman, et al. 2022. "One Stomatal Model to Rule Them All? Toward Improved Representation of Carbon and Water Exchange in Global Models." *Journal of Advances in Modeling Earth Systems* 14, no. 4: e2021MS002761.

Sack, L., and T. N. Buckley. 2016. "The Developmental Basis of Stomatal Density and Flux." *Plant Physiology* 171, no. 4: 2358–2363.

Sack, L., G. P. John, and T. N. Buckley. 2018. "ABA Accumulation in Dehydrating Leaves Is Associated With Decline in Cell Volume, Not Turgor Pressure." *Plant Physiology* 176, no. 1: 489–495.

Saliendra, N. Z., J. S. Sperry, and J. P. Comstock. 1995. "Influence of Leaf Water Status on Stomatal Response to Humidity, Hydraulic Conductance, and Soil Drought in *Betula occidentalis*." *Planta* 196: 357–366.

Santiago, L. S., G. Goldstein, F. C. Meinzer, et al. 2004. "Leaf Photosynthetic Traits Scale With Hydraulic Conductivity and Wood Density in Panamanian Forest Canopy Trees." *Oecologia* 140, no. 4: 543–550. https://doi.org/10.1007/s00442-004-1624-1.

Scoffoni, C., C. Albuquerque, T. N. Buckley, and L. Sack. 2023. "The Dynamic Multi-Functionality of Leaf Water Transport Outside the Xylem." *New Phytologist* 239, no. 6: 2099–2107.

Scoffoni, C., C. Albuquerque, H. Cochard, et al. 2018. "The Causes of Leaf Hydraulic Vulnerability and Its Influence on Gas Exchange in *Arabidopsis thaliana*." *Plant Physiology* 178, no. 4: 1584–1601.

Scoffoni, C., D. S. Chatelet, J. Pasquet-Kok, et al. 2016. "Hydraulic Basis for the Evolution of Photosynthetic Productivity." *Nature Plants* 2, no. 6: 1–8.

Scoffoni, C., and L. Sack. 2017. "The Causes and Consequences of Leaf Hydraulic Decline With Dehydration." *Journal of Experimental Botany* 68, no. 16: 4479–4496.

Sellin, A., and P. Kupper. 2005. "Variation in Leaf Conductance of Silver Birch: Effects of Irradiance, Vapour Pressure Deficit, Leaf Water Status and Position Within a Crown." *Forest Ecology and Management* 206, no. 1–3: 153–166.

Shackel, K. A. 1987. "Direct Measurement of Turgor and Osmotic Potential in Individual Epidermal Cells: Independent Confirmation of Leaf Water Potential as Determined by In Situ Psychrometry." *Plant Physiology* 83, no. 4: 719–722.

Sharpe, P. J. H., H. Wu, and R. D. Spence. 1987. "Stomatal Mechanics." In *Stomatal Function*, edited by E. Zeiger, G. D. Farquhar, and I. R. Cowan, 91–114. Stanford University Press.

Sicangco, C. K., M. E. Sabot, J. E. Drake, M. G. Tjoelker, and B. E. Medlyn. 2026. "Weighing the Options: A Test of Alternative Stomatal Optimisation Models at High Temperatures." *New Phytologist* 250, no. 3: 1551–1568.

Sinclair, T. R., M. A. Zwieniecki, and N. M. Holbrook. 2008. "Low Leaf Hydraulic Conductance Associated With Drought Tolerance in Soybean." *Physiologia Plantarum* 132, no. 4: 446–451. https://doi.org/10.1111/j.1399-3054.2007.01028.x.

Sperry, J. S., and D. M. Love. 2015. "What Plant Hydraulics Can Tell Us About Responses to Climate-Change Droughts." *New Phytologist* 207, no. 1: 14–27.

Sperry, J. S., M. D. Venturas, W. R. Anderegg, et al. 2017. "Predicting Stomatal Responses to the Environment From the Optimization of Photosynthetic Gain and Hydraulic Cost." *Plant, Cell & Environment* 40, no. 6: 816–830.

Sperry, J. S., Y. Wang, B. T. Wolfe, et al. 2016. "Pragmatic Hydraulic Theory Predicts Stomatal Responses to Climatic Water Deficits." *New Phytologist* 212, no. 3: 577–589.

Tor-ngern, P., R. Oren, E. J. Ward, S. Palmroth, H. R. McCarthy, and J. Domec. 2015. "Increases in Atmospheric CO_2 Have Little Influence on Transpiration of a Temperate Forest Canopy." *New Phytologist* 205, no. 2: 518–525.

Torres-Ruiz, J. M., H. Cochard, S. Delzon, et al. 2024. "Plant Hydraulics at the Heart of Plant, Crops and Ecosystem Functions in the Face of Climate Change." *New Phytologist* 241, no. 3: 984–999.

Tsuda, M., and M. T. Tyree. 2000. "Plant Hydraulic Conductance Measured by the High Pressure Flow Meter in Crop Plants." *Journal of Experimental Botany* 51: 823–828.

Urban, J., M. W. Ingwers, M. A. McGuire, and R. O. Teskey. 2017. "Increase in Leaf Temperature Opens Stomata and Decouples Net Photosynthesis From Stomatal Conductance in Pinus Taeda and *Populus deltoides* x Nigra." *Journal of Experimental Botany* 68, no. 7: 1757–1767.

von Caemmerer, S., T. Lawson, K. Oxborough, N. R. Baker, T. J. Andrews, and C. A. Raines. 2004. "Stomatal Conductance Does Not Correlate With Photosynthetic Capacity in Transgenic Tobacco With Reduced Amounts of Rubisco." *Journal of Experimental Botany* 55: 1157–1166.

Wang, Y., J. S. Sperry, W. R. Anderegg, M. D. Venturas, and A. T. Trugman. 2020. "A Theoretical and Empirical Assessment of Stomatal Optimization Modeling." *New Phytologist* 227, no. 2: 311–325.

Wedegaertner, K., A. Shekoofa, S. Purdom, K. Walters, L. Duncan, and T. B. Raper. 2022. "Cotton Stomatal Closure Under Varying Temperature and Vapor Pressure Deficit, Correlation With the Hydraulic Conductance Trait." *Journal of Cotton Research* 5, no. 1: 20.

Whalley, W., E. Ober, and M. Jenkins. 2013. "Measurement of the Matric Potential of Soil Water in the Rhizosphere." *Journal of Experimental Botany* 64, no. 13: 3951–3963.

Wilson, K. B., P. J. Hanson, P. J. Mulholland, D. D. Baldocchi, and S. D. Wullschleger. 2001. "A Comparison of Methods for Determining Forest Evapotranspiration and Its Components: Sap-Flow, Soil Water Budget, Eddy Covariance and Catchment Water Balance." *Agricultural and Forest Meteorology* 106, no. 2: 153–168.

Wolf, A., W. R. Anderegg, and S. W. Pacala. 2016. "Optimal Stomatal Behavior With Competition for Water and Risk of Hydraulic Impairment." *Proceedings of the National Academy of Sciences of the United States of America* 113, no. 46: E7222–E7230.

Wolfe, B. T., M. Detto, Y. Zhang, et al. 2023. "Leaves as Bottlenecks: The Contribution of Tree Leaves to Hydraulic Resistance Within the Soil–Plant–Atmosphere Continuum." *Plant, Cell & Environment* 46, no. 3: 736–746.

Wong, S. C., I. R. Cowan, and G. D. Farquhar. 1979. "Stomatal Conductance Correlates With Photosynthetic Capacity." *Nature* 282: 424–426.

Wood, J. D., M. Detto, M. Browne, et al. 2024. "The Ecosystem as Super-Organ/Ism, Revisited: Scaling Hydraulics to Forests Under Climate Change." *Integrative and Comparative Biology* 64, no. 2: 424–440.

Wullschleger, S. D. 1993. "Biochemical Limitations to Carbon Assimilation in C3 Plants—A Retrospective Analysis of the A/Ci Curves From 109 Species." *Journal of Experimental Botany* 44: 907–920.

Zailaa, J., S. Trueba, M. Browne, et al. 2025. "Sensitive Hydraulic and Stomatal Decline in Extreme Drought Tolerant Species of California Ceanothus." *Plant, Cell & Environment* 48, no. 2: 1555–1573.

Zeppel, M., D. T. Tissue, D. Taylor, C. Macinnis-Ng, and D. Eamus. 2010. "Rates of Nocturnal Transpiration in Two Evergreen Temperate Woodland Species With Different Water-Use Strategies." *Tree Physiology* 30: 988–1000.

Supporting Information

Additional supporting information can be found online in the Supporting Information section. **Figure S1:** Trends in midday leaf water potential under control conditions (a; daily max temperature 28°C–29°C) or during a four-day heatwave (b; daily max air temperature 43°C–44°C), measured for *Eucalyptus parramattensis* trees (black symbols; error bars are ± SE) or simulated by the new model (blue lines) or the USO model (red lines). Soil water had been withheld from both control and heatwave trees for 30 days prior to the experiment. Original data from Drake et al. (2018), with USO simulations from Sicangco et al. (2026) (cf. their figure 5). The heatwave was imposed from 31 October to 03 November (2016), corresponding to the first three water potential measurements shown here. **Figure S2:** Relationships of g_{sw} with VPD (a), residual photosynthetic capacity ($A_m - A$, (b)), and ambient CO_2 (c_a, (c)), for the three arid-environment species for which fitted values of E_m and p were several orders of magnitude larger than for other arid species. For *S. senegal*, g_{sw} was unrelated to VPD, and not because of countervailing influences of $A_m - A$ or c_a (b, c). For *E. aparrerinja*, VPD varied minimally in the dataset. For *E. terminalis*, $A_m - A$ increased strongly as VPD increased, and not because stomatal closure reduced assimilation rate (c_i, not shown, was nearly constant); this nullified the effect of Δw in the denominator of Equation (5), making stomata appear insensitive to VPD. Each of these patterns would cause the fitting algorithm to identify very large values for both E_m and p, equivalent to low VPD sensitivity. **Figure S3:** Figure 5 from the main text is reproduced here, in two forms: first (left) including all points (identical to Figure 5), and second (right), excluding the 13 points for which nls() in R could not successfully fit parameters for Equation (5), so estimates from a linear fit to an inverted form of the model were used instead, as described in Methods S3. None of the patterns are discernibly affected by exclusion or inclusion of those 13 points. This is the legend from Figure 5: Distributions of parameter values for the new model (in the form given by Equation (5), with parameters E_m and p) and the USO model (with parameter g_1) fitted to data of Lin et al. (2015), within various subgroupings as given by Lin et al.: (a–c) plant functional types ("savanna" refers to "savanna trees" as defined by Lin et al.); (d–f) latitudinal zones (as defined by Lin et al.); (g–i) gymnosperms vs. angiosperms; (j–l) regions of differing aridity. Medians are shown with vertical lines, and are also listed in Table S2, along with numbers of species × site combinations in each category and corresponding median adjusted r^2 values. **Table S1:** Model performance statistics for Dataset #1. Bolded values represent the highest performance for given species and parameter sets. In column 1, "different" means that each model was fitted separately for the control treatment and the drought treatment, so that there were two sets of parameters for each species; "same" means that each model was fitted to both treatments combined, so that there was only a single set of parameters for each species. **Table S2:** Mean parameters fitted for the new model (in the form given by Equation 5) and the USO model for Dataset #2. n: number of species × site combinations fitted in each group. r^2_{adj}: median adjusted correlation coefficient between observed and predicted g_{sw} across species × site combinations E_m, p, g_1: medians ± median absolute deviations. Units: E_m (mmol m^{-2} s^{-1}), p (nmol m^{-2} s^{-1}), g_1 ($kPa^{0.5}$).

Appendix A

A1.1: Biophysical Constraints and Biological Assumptions Underlying the BMF Model

Equation (3) is an adaptation of a process-based model (the "BMF" model; Buckley et al. 2003), which itself was derived by combining approximate descriptions of biophysical constraints and biological hypotheses. The BMF model was subsequently modified by Rodriguez-Dominguez et al. (2016); the modified version is discussed here. One biophysical constraint links stomatal conductance (g_{sw}) to the turgor pressures of guard and epidermal cells (P_g and P_e, respectively) (Buckley et al. 2003; DeMichele and Sharpe 1973; Edwards et al. 1976; Franks et al. 1998; Sharpe et al. 1987):

$$g_{sw} = \chi\left(P_g - (M+1)P_e\right), \tag{A1}$$

where χ is an empirical coefficient and M is the net mechanical advantage of the epidermis, which is positive in angiosperms (Edwards et al. 1976; Franks et al. 1998). Another biophysical constraint links P_g and P_e to leaf water potential (ψ_L) and to the osmotic gradient between guard and epidermal cells ($\delta\pi_g$): assuming epidermal cells are in approximate hydraulic equilibrium with the bulk leaf (Shackel 1987), and that guard cells are in hydraulic equilibrium with the epidermis, it follows that

$$P_g - (M+1)P_e = \left[\psi_L + \pi_g\right] - (M+1)\left[\psi_L + \pi_e\right] = \delta\pi_g - M\left(\psi_L + \pi_e\right), \tag{A2}$$

where π_g is guard cell osmotic pressure. A third biophysical constraint links ψ_L in turn to g_{sw}, via the latter's effect on transpiration rate, which drives water transport from the soil to the leaf:

$$\psi_L = \psi_s - \frac{g_{sw}\Delta w}{K}, \tag{A3}$$

where ψ_s is soil water potential, Δw is the leaf-to-air water vapor mole fraction difference, and K is soil-leaf hydraulic conductance. Equation A3 arises by combining Darcy's Law (soil-leaf flow = $K(\psi_s - \psi_L)$) with the assumption that soil-leaf flow is in steady-state with transpiration rate, E, which equals $g_{sw}\Delta w$.

The biological assumptions are that $\delta\pi_g$ is actively regulated in proportion to P_e and to the balance between energy production by the light reactions of photosynthesis and energy consumption by the Calvin cycle (Buckley 2005, 2019; Busch 2014; McAdam and Brodribb 2016; Mott 2009). In the BMF model, the latter effect was predicted using a biochemical model for mesophyll ATP concentration (denoted τ) derived by Farquhar and Wong (1984) from the photosynthesis model of Farquhar et al. (1980). Thus,

$$\delta\pi_g = \beta\tau P_e, \tag{A4}$$

where β is an empirical coefficient. Combining the constraints and assumptions described above eliminates water potential and turgor pressure from the system of equations, leading to the following model for stomatal conductance:

$$g_{sw} = \frac{\chi(\beta\tau - M)\left(\psi_s + \pi_e\right)}{1 + \chi(\beta\tau - M)\Delta w / K}. \tag{A5}$$

Although leaf water potential does not appear explicitly in this expression, it nevertheless remains an implicit variable, which varies over time along with g_{sw} itself; ψ_L can be calculated by applying the value of g_{sw} given by Equation (A5) to Equation (A3).

The BMF model thus required several parameters that were very difficult to estimate by experiment: χ, π_e, β, and three internal parameters in the ATP model (the total concentration of adenylates, the concentration of phosphorylation sites, and the potential RuBP pool size; see Buckley et al. (2003)). The original BMF model also assumed that guard cell osmotic pressure per se, rather than $\delta\pi_g$, was regulated in proportion to P_e and τ, which led to the inclusion of apoplastic osmotic pressure (π_a), and that water potential may be lower in guard cells than in epidermal cells due to flow of a fraction (f_g) of the transpiration stream through guard cells, through a resistance (r_{eg}); thus, in its original form, the BMF model also required π_a, f_g, and r_{eg} as inputs. Rodriguez-Dominguez et al. (2016) later introduced simplifications that eliminated the need for π_a, f_g, and r_{eg}.

A1.2: Solution of the New Model With Diffusional and Biochemical Constraints

Combining the new model for stomatal conductance (Equation 3 in the main text) with the diffusive constraint on CO_2 assimilation rate and the FvCB biochemical model for C_3 photosynthesis (Farquhar et al. 1980) leads to a cubic (3rd-order polynomial) expression for A. We derive that solution in Methods S1, and present the result here. We show in Methods S1 that there is never more than one root to the cubic for which $-R_d \le A < ¼J - R_d + b_o$ and $c_i > \Gamma_*$, where Γ_* is the photorespiratory CO_2 compensation point. Thus, the correct solution can be found by calculating roots until one satisfies the constraints that $-R_d \le A < ¼J - R_d + b_o$ and $c_i > \Gamma_*$; in general, only one root needs to be computed. For C_3 plants under carboxylation- or regeneration-limited conditions, the roots are given by

$$A_{[n]} = 2\sqrt{-\frac{Q_1}{3}}\cos\left(\frac{1}{3}\arccos\left(\frac{3Q_2}{2Q_1}\cdot\sqrt{-\frac{3}{Q_1}}\right) - \frac{2}{3}n\pi\right) - \frac{q_2}{3q_3} \text{ where } n \in [0,1,2], \tag{A6}$$

where [n] in the subscript is an index referring to the parameter n, and Q_1 and Q_2 are given by

$$Q_1 \equiv \frac{3q_3q_1 - q_2^2}{3q_3^2}, Q_2 \equiv \frac{2q_2^3 - 9q_3q_2q_1 + 27q_3^2q_0}{27q_3^3}, \tag{A7}$$

where q_0, q_1, q_2, and q_3 are coefficients of the cubic expression for A, given by

$$q_3 \equiv 1.6\Delta w + E_m r_{bc}, \tag{A8}$$

$$q_2 \equiv -E_m\left(c_a + S + r_{bc}(B + W)\right) - 1.6(p + \Delta w(B + W)), \tag{A9}$$

$$q_1 \equiv E_m\left(B\left(c_a + S\right) + ZW + r_{bc}BW\right) + 1.6W(p + \Delta wB), \tag{A10}$$

$$q_0 \equiv -E_m BZW, \tag{A11}$$

in which r_{bc} is the boundary layer resistance to CO_2, $E_m \equiv K\left(\psi_s - \psi_c\right)$, $p \equiv K/s$, $B \equiv {}^1\!/\!_4 J - R_d + b_o$, $Z \equiv c_a - \Gamma$; $W \equiv V_m - R_d$ or ${}^1\!/\!_4 J - R_d$, and $S \equiv K'$ or $2\Gamma_*$, when photosynthesis is limited by the rate of RuBP carboxylation or regeneration, respectively; $\Gamma \equiv \left(1 + R_d/W\right)\Gamma_* + \left(R_d/W\right)S$ is the CO_2 compensation point (distinct from Γ_*, the *photorespiratory* CO_2 compensation point), V_m is the maximum carboxylation velocity, K' is the effective Michaelis constant for carboxylation ($K' = K_c[1 + O/K_o]$, where K_c and K_o are the Michaelis constants for carboxylation and oxygenation, respectively, and O is the mole fraction of oxygen), R_d is non-photorespiratory CO_2 release rate, and c_a is ambient CO_2 mole fraction. There are four exceptions to the solution given above, corresponding to edge cases: (i) in darkness ($J = 0$), the solution is simply $A = -R_d$; (ii) if $\Delta w = 0$, the solution reduces to a quadratic, with the correct root given by $A = (1/2q_2)\left(-q_1 + (q_1{}^2 - 4q_0q_2)^{0.5}\right)$; (iii) if $b_o = 0$, then under regeneration-limited conditions, the solution also reduces to a quadratic, but with coefficients modified slightly: $A = (1/2q_2')\left(-q_1' - (q_1{}'^2 - 4q_0'q_2')^{0.5}\right)$, where $q_2' = q_3$, $q_1' = -E_m(c_a + S') - 1.6(p + \Delta wW)$, and $q_0' = E_m ZW$; and (iv) under triose phosphate utilization (TPU) limitation, the solution is simply $A = 3U - R_d$, where U is the TPU rate.

In C_4 species, using the Collatz et al. (1992) model for C_4 photosynthesis, the solution is also a cubic, but with the following coefficients:

$$q_3 \equiv 1.6\Delta w k_p + \left(\beta' + k_p r_{bc}\right)E_m, \tag{A12}$$

$$q_2 \equiv -\beta' M'' E_m - \left(M' - 2\beta' R_d\right)E_m - 1.6k_p\Delta w\left(M' - R_d\right) - k_p Y, \tag{A13}$$

$$q_1 \equiv M'' E_m\left(M' - 2\beta' R_d + k_p c_a\right) + R_d E_m\left(\beta' R_d - M'\right) + k_p Y\left(M' - R_d\right), \tag{A14}$$

$$q_0 \equiv -M''\left(R_d E_m\left(\beta' R_d - M'\right) + \left(M' - R_d\right)k_p c_a E_m\right), \tag{A15}$$

where k_p is the initial slope of the A vs c_i curve, M' is the CO_2-saturated photosynthetic rate (computed from light and carboxylation capacity; Equation S48), $M'' \equiv M' - R_d + b_o$, β' is the dimensionless curvature parameter for computing photosynthesis rate (P) as a hyperbolic minimum of CO_2-saturated and -limited rates (Equation S49), and $Y \equiv \left(c_a + rM''\right)E_m + 1.6\left(p + \Delta wM''\right)$. The correct root of the cubic in C_4 species is the smallest root that lies between $-R_d$ and $M' - R_d$. The full C_4 model and a derivation of the solution above are given in Methods S1. (Note that β', M' and M'' are unrelated to the parameters β and M in the BMF model.)

TABLE A1. List of parameter and variables used in this appendix and not in the main text.

Description	Symbol	Units	Default value
Quantum yield of CO_2 assimilation in C4 plants	α_c	CO_2/photon	—
Roots of cubic expression for A ($k \in [0,1,2]$)	A_k	$\mu mol\, m^{-2} s^{-1}$	—
Regeneration-limited CO_2 assimilation rate	A_j	$\mu mol\, m^{-2} s^{-1}$	—
Carboxylation-limited CO_2 assimilation rate	A_v	$\mu mol\, m^{-2} s^{-1}$	—
Composite parameter (${}^1\!/\!_4 J - R_d + b_o$)	B	$\mu mol\, m^{-2} s^{-1}$	—
Curvature parameter for C_4 photosynthetic co-limitation	β'	—	0.93
Fraction of transpiration that flows through guard cells	f_g	—	—
Initial slope of response of J to light	ϕ_j	electron/photon	[a]
Total photosynthetic CO_2 compensation point	Γ	$\mu mol\, mol^{-1}$	—
Photosynthetic photon flux density (PPFD)	i	$\mu mol\, m^{-2} s^{-1}$	—
Electron transport capacity (at 25°C)	$J_{m(25)}$	$\mu mol\, m^{-2} s^{-1}$	$1.7 \times V_{m(25)}$
Michaelis constant for RuBP carboxylation	K_c	$\mu mol\, mol^{-1}$	—
Michaelis constant for RuBP oxygenation	K_o	$\mu mol\, mol^{-1}$	—
Initial slope of A vs. c_i curve in C4 plants	k_p	$mol\, m^{-2} s^{-1}$	—
CO_2-saturated photosynthesis rate in C4 species	M'	$\mu mol\, m^{-2} s^{-1}$	—
$M' - R_d + b_o$	M''	$\mu mol\, m^{-2} s^{-1}$	—

TABLE A1 | (Continued)

Description	Symbol	Units	Default value
Index of cubic root	n	—	—
Ambient oxygen mole fraction	O	$\mu mol\ mol^{-1}$	—
Composite parameter used in cubic solution	P	$[\mu mol\ m^{-2}\ s^{-1}]^2$	—
Apoplastic osmotic pressure	π_a	MPa	—
Guard cell osmotic pressure	π_g	MPa	—
Composite parameter used in cubic solution	Q	$[\mu mol\ m^{-2}\ s^{-1}]^2$	—
0th-order coefficient in cubic expression for A	q_0	$[\mu mol\ m^{-2}\ s^{-1}]^2$	—
1st-order coefficient in cubic expression for A	q_1	$\mu mol\ m^{-2}\ s^{-1}$	—
2nd-order coefficient in cubic expression for A	q_2	—	—
3rd-order coefficient in cubic expression for A	q_3	$[\mu mol\ m^{-2}\ s^{-1}]^{-1}$	—
0th-order coefficient in quadratic expression for A if $b_o = 0$ [r]	q_0'	$\mu mol\ m^{-2}\ s^{-1}$	—
1st-order coefficient in quadratic expression for A if $b_o = 0$ [r]	q_1'	—	—
2nd-order coefficient in quadratic expression for A if $b_o = 0$ [r]	q_2'	$[\mu mol\ m^{-2}\ s^{-1}]^{-1}$	—
Curvature of smoothing between A_v and A_j	θ_A	—	0.99
Curvature parameter for response of J to light	θ_j	—	[a]
Hydraulic resistance from epidermal to guard cells	r_{eg}	$[mmol\ m^{-2}\ s^{-1}\ MPa^{-1}]^{-1}$	—
Generalized effective Michaelis constant (K' [c] or $2\Gamma_*$ [r])	S	$\mu mol\ mol^{-1}$	—
Triose phosphate utilization rate	U	$\mu mol\ m^{-2}\ s^{-1}$	—
Carboxylation capacity (at 25°C)	$V_{m(25)}$	$\mu mol\ m^{-2}\ s^{-1}$	50
Composite parameter ($V_m - R_d$ [c] or $J - R_d$ [r])	W	$\mu mol\ m^{-2}\ s^{-1}$	—
Composite parameter ($c_a E_m + 1.6(k + \Delta w M')$)	Y	$\mu mol\ mol^{-1}$ $mmol\ m^{-2}\ s^{-1}$	
Ambient CO_2 minus CO_2 compensation point ($c_a - \Gamma$)	Z	$\mu mol\ mol^{-1}$	—

Note: "[c]," "[r]," and "[t]" refer to values that apply under carboxylation, regeneration, and TPU-limited conditions, respectively.
[a]ϕ_j and θ_j were calculated from temperature following Bernacchi et al. (2003).